An assessment of reef coral calcification over the late Cenozoic

Thomas Brachert, Thierry Corrège, Markus Reuter, Claudia Wrozyna, Laurent Londeix, Philipp Spreter, Christine Perrin

Earth-Science Reviews 204 (2020) 103154

Contents lists available at ScienceDirect

Earth-Science Reviews

journal homepage: www.elsevier.com/locate/earscirev

An assessment of reef coral calcification over the late Cenozoic

Thomas C. Brachert[a,*], Thierry Corrège[b], Markus Reuter[a], Claudia Wrozyna[a], Laurent Londeix[b], Philipp Spreter[a], Christine Perrin[c]

[a] Universität Leipzig, Institut für Geophysik und Geologie, Talstrasse 35, 04103 Leipzig, Germany
[b] Université de Bordeaux / UMR 'EPOC' CNRS 5805, Allée Geoffroy St-Hilaire, CS 50023, 33615 Pessac cedex, France
[c] Département Homme et Environnement, Muséum National d'Histoire Naturelle, HNHP UMR7194, Centre Européen de Recherche en Préhistoire, Avenue Léon-Jean Grégory, 66720 Tautavel, France

ARTICLE INFO

Keywords:
reef coral
calcification rate
ocean acidification
geological past
Neogene
Quaternary

ABSTRACT

Shallow-water reef-building corals have an extensive geological record and many aspects of their evolution, biodiversity, and biogeography are known in great details. In contrast, the adaptive potential and risk of extinction of coral reefs in response to excessive warming and ocean acidification remains largely undocumented. It is well established that anthropogenic CO_2 emissions cause global warming and ocean acidification (lowering of pH), which increasingly impede the biomineralization process in many marine calcareous biota. The "light-enhanced" calcification machinery of the shallow-water reef corals is particularly threatened by this development through the combined effect of a lowering of the supersaturation of seawater with $CaCO_3$ (aragonite) and an expulsion of the symbiotic zooxanthellae (bleaching). The bleaching is of prime importance, because it interrupts the supply of DIC and metabolites required for pH upregulation within the calcification fluid. The degree of calcification in scleractinian reef corals may therefore represent a suitable tracer to assess the state of the ocean carbonate system and the photosynthetic performance of the zooxanthellae during past episodes of natural environmental change. This study presents the first comprehensive set of calcification data from reef corals covering the early Miocene to early Pleistocene interval (20.8 to 1.2 million years, Ma). Various screening procedures ensured that the studied coral skeletons are pristine and suited to yield meaningful stable isotope data ($\delta^{18}O$, $\delta^{13}C$) and calcification records. $\delta^{18}O$ and $\delta^{13}C$ values document growth environments consistent with current tropical and subtropical settings. To assess fossil calcification rates, we use a reference dataset of recent corals from the Indo-Pacific (*Porites*) and an independent validation dataset from the Western Atlantic-Caribbean (*Orbicella*). Almost all fossil corals document very low annual rates of upward growth (extension rate) relative to present, and lower skeletal bulk density than predicted by established modern relationships. To allow for a quantitative assessment of coral calcification performance, we use a new approach that we term the calcification anomaly. It is insensitive to sea-surface temperature and well-suited for comparative assessments of calcification performance between reef sites and over time. Based on this approach, the majority of fossil corals in our dataset displays hypo-calcification, while a few show optimal calcification and none display hyper-calcification. Compared to present-day growth conditions, the fossil calcification data show that (1) skeletogenesis responded in a fully compatible way to known environmental stresses (e.g. turbid water, elevated salinity, eutrophy), and that (2) the calcification performance within the reef window (i.e. oligotrophic clear-water settings) remained below that of modern z-corals. Since fossil coral $\delta^{13}C$ values are compatible with those of modern reef corals, we infer that the light-enhanced calcification system of symbiotic scleractinian corals was fully established by the beginning of the Neogene and that lower-than-present calcification performance was the likely response to a chronically low pH and/or low carbonate saturation state of the global ocean. If so, the present-day saturation state appears to be rather an exception than the norm and probably not a suitable starting point for predicting future calcification trends. In addition, using trends from the geological past for predicting future developments does not consider anthropogenic side-effects such as eutrophication and pollution.

* Corresponding author.
E-mail address: brachert@uni-leipzig.de (T.C. Brachert).

https://doi.org/10.1016/j.earscirev.2020.103154
Received 14 October 2019; Received in revised form 9 March 2020; Accepted 10 March 2020
Available online 16 March 2020

1. Introduction

Biogenic carbonate buildups and shallow-water reefs have an extensive geological record. Thanks to their economic significance as petroleum reservoir, the fundamentals of their sedimentary architecture, facies distributions, paleontological makeup and diagenesis, as well as their spatial distributional patterns and evolutionary traits in the Phanerozoic record are well described (James, 1983; Kiessling et al., 2002; Schroeder and Purser, 1986; Wilson, 1975; Wood, 1999). The modern scleractinian – coralline algal reef did not appear before the mid Cretaceous, although scleractinian corals have a long-lasting history from the Triassic onward. The first scleractinians appeared during the middle Triassic 240 million years (Ma) ago and shortly after became members, albeit not dominant, of shallow-water reefs. Following an adaptive radiation during the late Triassic, scleractinians became for a first time constructional in forming large patch reefs before they were strongly decimated again during the Triassic/Jurassic extinction event 201 Ma (Flügel, 2002; Stanley, 2003).

A coral reef gap of 14 million years duration existed during the early Triassic following the extinction of all Paleozoic anthozoans by the end of the Permian (Flügel, 2002; Stanley, 2003). Given high mid Triassic skeletal variability and taxonomical diversity, the origin of the scleractinians remains unclear, however. Molecular phylogenetic data suggest the divergence of the main morphological clades to have occurred well before the first appearance of the scleractinians during the mid Triassic, but an ancestry from the Paleozoic anthozoans, Rugosa and Tabulata, is highly unlikely (Kitahara et al., 2010; Romano and Cairns, 2000; Romano and Palumbi, 1996; Stanley, 2003). Since the absence of scleractinians from rocks older than middle Triassic is unlikely to be owed to an observational artefact, an origin from originally soft-bodied, sea anemone-like creatures and a polyphyletic origin of the scleractinian skeleton is generally considered the most likely. Nonetheless, beyond the absence of scleractinian fossils of elder-than-mid Trassic age, reef gaps have been reported also from the early Cenozoic (Budd, 2000; Perrin, 2002). The loss of coral reef volumes and their replacement by larger-foraminifer carbonates during the early Paleogene PETM (Paleocene-Eocene Thermal Maximum, 56 Ma) and Eocene are perhaps the globally most incisive interruptions in their record and evolution (Plaziat and Perrin, 1992; Wilson and Rosen, 1998). Although higher-than-present sea-surface temperatures (SSTs) may have been an important control for shallow-water reef corals and coral reef declines, calcification crises caused by ocean acidification (OA) are the most commonly accepted hypothesis (Kiessling and Simpson, 2011; Scheibner and Speijer, 2008). Calcification experiments with modern reef-building corals have shown that they can survive periods of more acidic conditions than present as solitarian, non-skeletal, sea anemone-like creatures that restart forming colonies and precipitating skeletons when transferred to normal pH conditions again (Fine and Tchernov, 2007). Thus, the process of decalcification / calcification is reversible, and we suggest the degree of calcification of coral skeletons might represent a semi-quantitative tracer for the shallow-marine calcification environment, either controlled by global seawater saturation with aragonite, seawater pH or various more local, stressors of nearshore growth environments.

Here, we review the first comprehensive dataset of calcification records from fossil shallow-water reef corals. It includes corals from 16 time-slices dated from 20.8 to 1.2 Ma that are in an excellent state of preservation and allow for the measurement of environmental proxy data (oxygen and carbon stable isotopes: $\delta^{18}O$, $\delta^{13}C$) and calcification variables (growth rate, skeletal bulk density, calcification rate). To account for temporal and regional SST and calcification trends, we use recalibrated stable isotope values and normalized calcification rates, and discuss possible driving mechanisms behind distinct under- or over-calcification (hypo- and hyper-calcification). For a calibration of calcification performance relative to the optimum, we use a reference dataset based on recent reef corals from the Indo-Pacific (IP) and an independent validation dataset from the Western Atlantic and Caribbean (WA-C) that both include growth data from the optimal reef growth window and stressed environments (e.g. freshwater influx and elevated salinity, high turbidity, CO_2 seeping). On this basis, we discuss whether hypo-calcification during the past was an effect of generally lower calcification potentials (e.g. taxonomically controlled) or a response to local and global environmental stresses.

1.1. Overview of skeletogenesis in shallow-water reef corals

During skeletogenesis (Al-Horani, 2016), scleractinian shallow-water reef corals extract dissolved inorganic carbon (DIC) together with Ca^{2+} ions from seawater to rapidly precipitate calcium carbonate ($CaCO_3$) in the form of metastable aragonite. As reviewed by McCulloch and co-workers (McCulloch et al., 2017), this process involves an exchange mechanism of ions with the calcifying fluid (CF) via Ca-ATPase. In this way, protons (H^+) of the CF are exchanged by Ca^{2+} ions. Calcification from this seawater-derived fluid occurs within a small compartment between the aboral tissue of the polyp and the extracellular mineralization front of the skeleton through elevating the pH (by removal of H^+) and metabolic addition of DIC. In this reaction, carbonic anhydrases further catalyse the conversion of CO_2 to HCO_3^-. This process leads to an overall upregulation of pH (+0.2 to +0.5 units), saturation state of CF with $CaCO_3$ (x5) and DIC (x2 to x3) relative to seawater. An important process boosting these complex reactions has been identified as "light-enhanced calcification" (Goreau, 1959). The photosynthetic activity of certain endosymbiotic, unicellular dinoflagellates (zooxanthellae, thus "z-corals") provides both, energy and carbon, to support the biomineralization process. Consequently, the calcification process displays an annual signature due to seasonal changes in solar insolation and SST. The highest DIC occurs during summer and responds to an enhanced thermal delivery of carbon derived from zooxanthellate photosynthesis. In contrast, the highest pH of the CF occurs during periods of low DIC in winter. These mutualistic patterns of DIC and pH grant for the maintenance of high supersaturation with $CaCO_3$ in the CF over the entire year – a key aspect of skeletal calcification. Nonetheless, the spatial disconnection of the zooxanthellae situated within the oral tissue from the calcioblastic, aboral tissue of the polyp remains a problem to the model (McCulloch et al., 2017) (Fig. 1). Although the precise mechanisms by which calcification in z-corals is enhanced by symbiont photosynthesis is not completely understood, the topic has great relevance to understanding the links between global warming and coral bleaching in the present and past (Stanley Jr and van de Schootbrugge, 2018).

On a microscopic scale, skeletal accretion involves rapid upward growth and successive secondary thickening of previously formed skeletal structures, which altogether reflects a complex interplay of inorganic and biological processes at molecular level. An extensive up-to-date review of patters and processes of scleractinian skeletogenesis has been presented recently by Drake et al. (2020). Simplified speaking, rapid accretion occurs by aggregates of nanometer-sized, granular crystals termed Rapid Accretion Deposits (RAD), or Centers of Calcification (COC) in an alternate terminology (Stolarski, 2003). Spatially more or less disconnected from the COCs is a zone where thickening of the COC regions takes place by extensive deposition of aragonite fibers, generally called thickening deposits (TD) (Stolarski, 2003). The thickening stops when the fiber crystals are no longer in contact with the calcioblastic tissue, which rhythmically retracts from deeper zones of the skeleton during upward growth of the coral colony. Under the assumption of a uniform thickness of the mineralizing tissue, high (low) rates of accretion in an upward direction allow less (more) time for thickening and will result in low (high) skeletal bulk density (Barnes and Lough, 1993; Lough and Barnes, 2000).

On a macroscopic scale, X-radiographs of slices of most corals with a massive growth form display rhythmic, dark and light bands known as density bands that reflect seasonal growth changes (Knutson et al.,

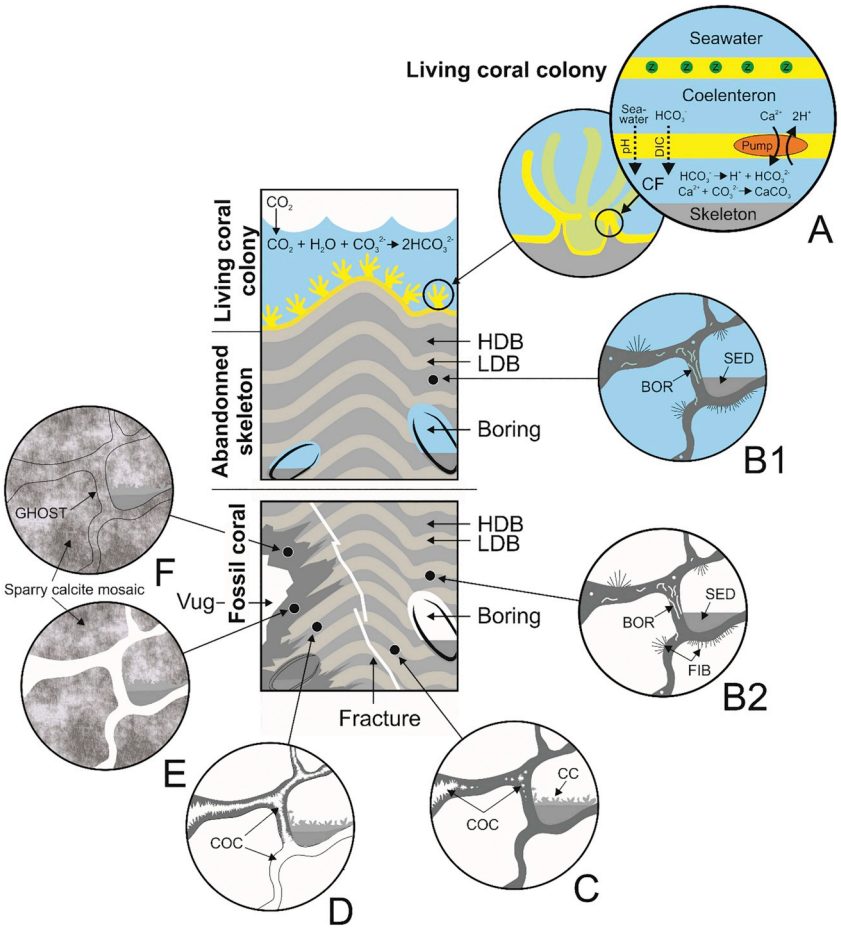

Fig. 1. Schematic representation of a living z-coral colony and a fossil corallum (skeleton of a z-coral colony). The living colony forms a thin tissue layer on top of a porous, more or less hemispherical skeleton. The tissue rhythmically retracts from previously formed skeleton upon continued upward growth of the coral colony. The abandoned part of the skeleton displays discrete annual growth bands, expressed as bands of high and low density in X-radiographs (HDB, LDB), as well as various borings or shells of endolithic and ingrown biota. The fossil skeletons display the same set of characteristics but are commonly further modified by freshwater and burial diagenesis (C – F). Depending on the degree of freshwater diagenesis, the skeletons may display open or cemented fractures, patches of sparry calcite and large vugs formed by dissolution. Yellow = living tissue; Light blue = seawater; White = air-filled porosity. A: The calcification mechanism involves an upregulation of pH, DIC and supersaturation of $CaCO_3$ relative to seawater. The oral tissue contains the zooxanthellae (green), the aboral tissue comprises the calcioblastic cells with the ATPase pumps (orange). Simplified from McCulloch et al. (2017). B – F: Schematic microscopic views of skeletal textures; the textures shown from B through F do not necessarily imply a continuous trend of increasing diagenetic alteration. B1: The abandoned skeleton below the living colony is infested by macro- and microendoliths (BOR) and affected by inorganic marine cementation (FIB). Some internal sediments (SED) may occur forming geopetal fabrics within macroborings and above skeletal structures, e.g. tabular dissepiments. B2: Fossil skeleton in a pristine preservation. Alteration textures are the same as in B1 and not modified by freshwater diagenesis. C: Some dissolution has occurred along the zones of rapid skeletal accretion, termed centers of calcification (COC). Patches of rhombohedral calcite (CC) may occur. D: Dissolution at COCs is intense and has caused hollow, tube-like skeletal structures, typically within HDBs. E: Freshwater sparry calcite cement preferentially infills primary skeletal porosity, while the original skeleton forms moldic porosity. Sparry calcite preferentially follows the HDBs. This type of `negative´ preservation is typical to the record of Neogene reefs in many regions. Large vuggy porosity may remain within the center of the corallum. F: Entire skeleton replaced by sparry freshwater cements. Some ghost structures (GHOST) of the original skeleton remain within mosaics of equant calcite.

1972) (Fig. 1, Plate S10–S16). Counting couplets of bands of high and low density (high density band or HDB, low density band or LDB) and annual cycles of oxygen isotope ratios ($\delta^{18}O$) as a proxy for SST give consistent results. Thus, one couplet of density bands and one cycle of $\delta^{18}O$ are generally the expression of one year of growth, and the HDB and LDB can be shown to represent the cool and warm season, respectively (Felis and Pätzold, 2004). In addition to growth bands recording regular seasonal growth cyclicity, well-developed additional bands may re-occur on a regular basis. For instance, massive *Porites* from the Arabian Sea (Oman) display an additional HDB within the warm-season LDB due to surface-water cooling during upwelling of the SW-monsoon termed double HDB (Tudhope et al., 1996). A doublet of HDBs and LDBs per year has been suggested to occur also, if SSTs at a growth site fluctuate around the calcification optimum (Brachert et al., 2013; Worum et al., 2007). Regular, sub-annual microbands reflecting lunar cycles exist also (DeCarlo and Cohen, 2017). In contrast, thin bands of exceptionally high density may occur rather erratically within the LDB documenting periods of stress (stress bands), e.g. bleaching events (Hudson et al., 1976), while further complications of the banding patterns and chronologies relate to missing beats (no growth) in records, individual traits in growth rhythms, or technical artefacts (Benson et al., 2019; Booker et al., 2019).

A combination of the banding patterns and $\delta^{18}O$ cycles with carbon stable isotope data ($\delta^{13}C$) bears additional significant information on the coral´s annual heterotrophy/phototrophy metabolism and growth environment. $\delta^{13}C$ signatures are often not straightforward to interpret, however, and typical complications may result from discharges of freshwater with isotopically negative carbon, oxidation of organic matter or variable algal photosynthesis and productivity (Swart et al., 1996). Nonetheless, coral sclerochronologies including also data from other isotope systems (e.g. $\delta^{11}B$, $\Delta^{14}C$) and geochemical proxy records (e.g. Sr/Ca, B/Ca) can provide detailed information on current and past climate variability and global change (Felis and Pätzold, 2004; McCulloch et al., 2017).

1.2. Current threats for shallow-water reef-building corals by rising atmospheric pCO_2

Current global environmental change increasingly endangers the z-corals of the tropical- subtropical shallow-water reefs in a wide range of ways. Among these, anthropogenic carbon dioxide (CO_2) emissions are perhaps the most severe, because they negatively interfere with the environment of coral growth in at least two different ways: (1) The emissions induce warming of sea-surface temperatures, which increases the risk of bleaching events, i.e. the release of zooxanthellae (Glynn, 1983; Stanley Jr and van de Schootbrugge, 2018). The bleaching disrupts the internal nutrient recycling between the coral host and zooxanthellae as well as metabolic supply of DIC and metabolites necessary to upregulate the pH of the calcifying fluid (McCulloch et al., 2017). Hence, warming-induced bleaching constitutes a significant threat to the growth of shallow-water reef corals. (2) Increasing atmospheric pCO_2 affects the marine carbonate system, because a substantial portion of the emissions is being absorbed by the ocean, a process termed Ocean Acidification (OA) (Hönisch et al., 2009). The CO_2 uptake by the surface-ocean drives the oceanic carbonate system to lower pH and decreased saturation with respect to calcium carbonate minerals. The

saturation state of seawater of the metastable aragonite ($\Omega_{aragonite}$) forming the coral skeleton is described as the product of the concentrations of the Ca^{2+} and CO_3^{2-} ions divided by the stoichiometric solubility product of aragonite at a specified temperature, salinity and pressure (Cyronak et al., 2016; Kleypas et al., 1999a). It is generally acknowledged that OA negatively impacts skeletal biomineralization in corals, whereby no complete agreements exists whether this is an effect of increasing seawater [H^+] or decreasing [CO_3^{-2}] with a concomitant lowering of $\Omega_{aragonite}$ (Cyronak et al., 2016; De'ath et al., 2009; Gattuso et al., 1998). In modern seawater, [Ca^{2+}] is near conservative and any variation in $\Omega_{aragonite}$ is determined by changes in [CO_3^{-2}]. While $\Omega_{aragonite}$ is high and constant at open ocean reefs, nearshore shallow-water reef settings are subject to substantial, local $\Omega_{aragonite}$ variations through evaporation, freshwater influx and carbon cycling. This local $\Omega_{aragonite}$ variability at various time-scales tends to fully mask the effects of global OA and carbonate saturation decline (Hofmann et al., 2011).

Additional effects of global environmental change concern an increase in the number and intensity of tropical storms with a higher destructive power on reefs. The associated intensified rainfall brings more sediment discharges and nutrients to nearshore coral environments (Riegl et al., 2009). Although nutrients are essential to the growth of all organisms, increasing eutrophication paradoxically has a negative net effect on the carbonate balance of a reef. In fact, high nutrients stimulate the growth of plankton what causes a shallowing of the euphotic depth and thus a narrowing of the depth range of z-corals and calcareous algae, i.e. less carbonate production. In addition, nutrients favor the growth of fast growing non-calcified algae and non-constructional suspension feeders, which additionally displace the slow growing constructional corals and calcareous algae. Among the fast growing competitors are also many bioeroders that further affect the labile equilibrium between construction and destruction of a reef (Hallock and Schlager, 1986). Nonetheless, the combined effects of all of these stressful growth conditions – either global or more local – on the reef biota and carbonate sedimentary systems remain poorly known, also because of opposing effects on the competing communities of fleshy algae and constructional corals and calcareous algae in their struggle for light and space (Fabricius et al., 2011; Ries et al., 2009; Veron, 2000).

1.3. The reef window model: template for the geological past

Most present-day coral reefs occur in open waters protected from terrestrial inputs, where $\Omega_{aragonite}$ range between 3.4-4.1, winter SSTs do not fall below 18 °C, salinity is normal marine, solar irradiation is sufficiently high to support photosynthesis of the symbiotic zooxanthellae, while the concentration of nutrients is generally low (Kleypas et al., 1999a; Veron, 2000). Beyond this optimal reef growth environment, z-corals can grow at slightly lower SSTs (SST_{annual} 11 to 14 °C) and $\Omega_{aragonite}$ (< 3.5) as level-bottom coral communities without forming frameworks (Guinotte et al., 2003; Kleypas et al., 1999b; Veron, 2000). The apparently paradoxical situation that coral reefs flourish mostly in oligotrophic regions of the ocean was already noted by Darwin as the reef paradox (Darwin, 1842) and later recognized as the "reef growth window" (James and Bourque, 1992). Within the blue waters of the reef growth window, the reef-building or "hermatypic" coral – zooxanthellae – symbiotic system runs at optimum efficiency because of its capability for recycling the sparse nutrients available and little competition for space and light with encrusting heterotrophs and non-calcified algae that require higher amounts of nutrients to grow (Hallock and Schlager, 1986). Apart from light-enhanced calcification through symbiont photosynthesis (Goreau, 1959), the main stimulus for skeletal carbonate production by corals and other mixotrophs is SST (McCulloch et al., 2017). SST has a positive linear effect on upward skeletal growth (extension rate) and calcification rates but a negative effect on skeletal bulk density in corals (Lough and Cooper, 2011). For this reason, accurate predictions of calcification rates for corals from the reef growth window can be made for any extension rate or SST (Lough and Barnes, 2000), a pattern further on termed optimal calcification. Optimal calcification does not refer to the theoretical maximum calcification rate of any given taxon of z-coral, i.e. its calcification potential, but to its predictable maximum calcification performance at any given SST regime within the reef growth window. However, increasing evidence exists for a non-linear relationship of z-coral growth with SST and a suggested maximum of calcification to occur at 26-27 °C annual temperature, beyond which the growth response of corals to SST has a negative slope (Lough and Cooper, 2011; Worum et al., 2007).

1.4. Reefs of the late Cenozoic: Parallels with climate and seawater quality

From the earliest Miocene onwards (23 Ma), shallow marine carbonate platforms and coral reefs spread to higher northern latitudes than today because of globally warmer climates and smaller latitudinal SST gradients (Perrin, 2002). From approx. 23 to 6 Ma, the northern limit of the global reef belt was relatively stable at ~40°N paleolatitude (Perrin and Kiessling, 2010). A significant northward expansion of the reef belt occurred during the Middle Miocene Climatic Optimum (MMCO), 17 to 14 Ma ago, when it reached ~50°N paleolatitude (Perrin and Kiessling, 2010). Parallel with substantial global cooling at 6 Ma, the northern margin of the global reef belt stepped towards the equator at ~20°N, before it gradually took in its present position at ~30 °N (Lear et al., 2015; Perrin and Kiessling, 2010; Zachos et al., 2001). High-frequency oscillations of the reef belt superimposed on this long-term trend have been documented for the late Miocene (10 – 5 Ma) and are particularly well established for the late Quaternary glacial – interglacial climate changes (0.1 to 0 Ma) (Blanchon, 2011; Brachert et al., 1996; Brachert et al., 2006b).

For most of the Neogene and Quaternary, the oceanic carbonate system maintained high saturation with calcium carbonate in spite of high pCO_2 due to various weathering feedbacks, e.g. alkalinity brought in by rivers (Kump et al., 2009; Pälike et al., 2012). Nonetheless, during the MMCO, pCO_2 reached a maximum of 470–630 ppm that caused seawater pH and $\Omega_{aragonite}$ to attain the smallest values of the entire Neogene and Quaternary (Sosdian et al., 2018). The values of pH = 7.6 and $\Omega_{aragonite}$ = 2.5–3.5 inferred for low latitudes were below known present-day thresholds for coral reef development, however (Kleypas et al., 1999b; Sosdian et al., 2018; Veron, 2000). Two other high pCO_2 periods dated ~9 and ~3 Ma, respectively, are also likely candidates for periods of globally low pH and $\Omega_{aragonite}$ (Seki et al., 2010; Sosdian et al., 2018). Increasing variability of pH and $\Omega_{aragonite}$ interfering with carbonate production is also likely to have occurred upon the intensification of the Northern Hemisphere (NH) glaciation dynamics between 2.9 and 2.4 Ma ago that culminated during the last glacial – interglacial cycle (Hönisch et al., 2012; Pälike et al., 2012; Raymo, 1994). At least for the latter it has been suggested to have induced changes in calcification of the calcareous plankton (Barker and Elderfield, 2002; Beaufort et al., 2011), while no clear evidence for earlier Cenozoic calcification changes has been presented (Kump et al., 2009).

1.5. Reef diagenesis

Coral calcification records from deep geological time are unusual, because the porous aragonitic skeletons of scleractinian corals normally undergo rapid alteration. The process starts already in vivo below the living tissue (Enmar et al., 2000; Perrin and Cuif, 2001; Perrin and Smith, 2007) and continues post-mortem because the highly porous coral skeletons and reefal carbonates form a geochemically open system. Upon contact with meteoric fluids, the metastable aragonite of the coral skeletons and many other calcareous biota (e.g. mollusks, green algae) are subject to rapid alteration into stable calcite during

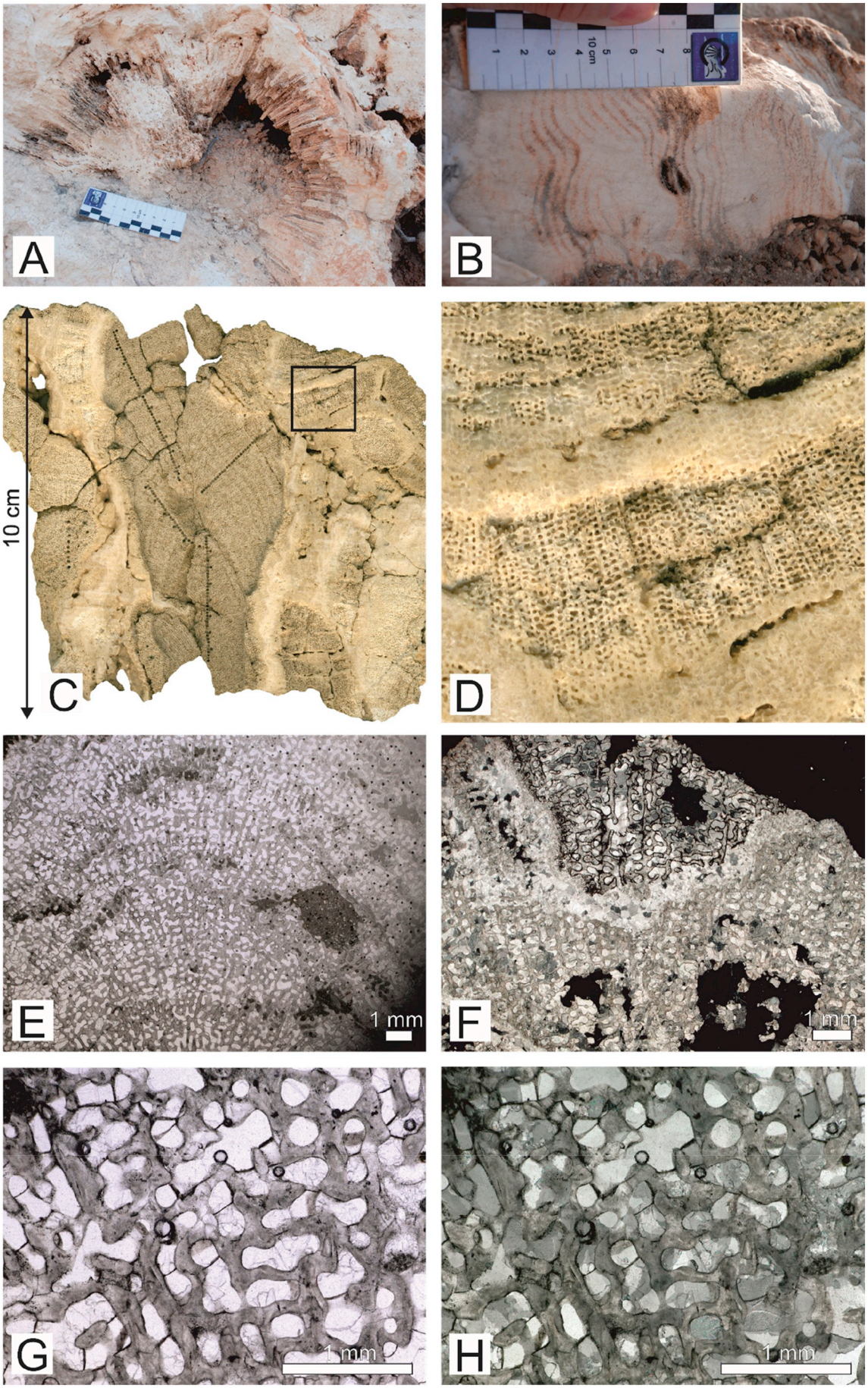

(caption on next page)

Plate 1. Diagenetic alteration of scleractinian coral skeletons: Field and thin-section aspects.
Figure A: Weathering aspect of a massive, undetermined z-coral from limestone outcrop. In an outer zone, the coral is fully transformed into sparry calcite; the central portion of the former skeleton forms a large open vug. Pakhna Formation, early Miocene, southern Cyprus.
Figure B: Fragment of massive *Porites*, which is fully replaced by blocky calcite spar. Large central hollow likely represent a vug formed by dissolution. According to ghost structures of the annual density bands, mean annual extension rate was approximately 0.4 cm per year. Pakhna Formation, early Miocene, southern Cyprus.
Figure C: Massive *Porites* displaying patchy diagenetic alteration. A pristine zone (primary aragonite, open skeletal porosity) in the center of the fragment is sourrounded by skeleton subject to variable degrees of dissolution and cementation. Black frame shows position of (D). Agia Varvara Formation, late Miocene, Crete (Moni Gorgolaini, MG 24-2).
Figure D: Close-up from (C) showing alternating bands of complete transformation into sparry calcite with preserved ghost structures of the original skeleton (center), elongate vugs following the growth bands, and bands showing linings of blocky calcite cement and molds after the original skeleton. All in all, the original annual bands remain preserved in this specimen. Agia Varvara Formation, late Miocene, Crete (Moni Gorgolaini, MG 24-2).
Figure E: Skeleton of massive *Porites*. Except for elongate patches of microcrystalline carbonate infilling intra-skeletal porosity and borings, most original porosity is still open, while the aragonite of the skeleton is fully replaced by blocky calcite spar. Black dots = air bubbles. Thin-section micrograph, plane light, Ambelousos Formation, late Miocene, Crete (Psalidha, P-GPS225).
Figure F: Peripheral zone of the massive *Porites* shown in (E). Various types of skeletal preservation coexist at small spatial scales: Within the center, a mosaic of blocky calcite spar prevails that seals vuggy porosity without preserving any ghost strucuture of the original skeleton. Below is a zone showing ghost structures of the skeleton within sparry calcite and irregular, open vugs (black patches). Near the top of the micrograph is a region with open vugs (black patches) and relicts of the skeleton being clearly marked by black outlines. The black outlines are thin empty spaces resulting from the dissolution of aragonite relicts of the skeleton at a very late stage of diagenesis. Crossed nicols, Ambelousos Formation, late Miocene, Crete (Psalidha, P-GPS225).
Figures G and H: Thin-section micrograph of massive *Porites*. The skeleton and intra-skeletal porosity is fully is replaced / infilled by blocky calcite spar. (G): Plane light, (H): crossed nicols. Ambelousos Formation, late Miocene, Crete (Psalidha, P-GPS225).

limestone diagenesis (Dullo, 1984; Schroeder and Purser, 1986). This process of alteration comprises neomorphism, dissolution and cementation, and leads to a complete loss of any original environmental information archived in the skeletons (Fig. 1, Plate 1/A–H). Nonetheless, single well-preserved coral fossils have been reported in the literature from rare examples of diagenetically closed systems and represent excellent, albeit isolated, archives for sub-annually and inter-annually resolved proxy data and calcification records (Brachert et al., 2006a; Brachert et al., 2016a; Brachert et al., 2016b; Denniston et al., 2008; Frankowiak et al., 2016; Mackenzie et al., 1997; Mertz-Kraus et al., 2009b; Stolarski, 2003; Stolarski et al., 2016; Watanabe et al., 2011; Weiss et al., 2017; White et al., 2008) (Fig. 1/B2, Plate 2/A–I).

2. Terminologies, materials and methods

2.1. Terminologies

Settings within the reef growth window have been classified between “optimal” and “marginal” with regard to a particular regime of water chemistry, temperature and solar irradiation (Done, 2011; Guinotte et al., 2003; Kleypas et al., 1999b). In this contribution, we refer to coral reefs formed in shallow water by z-corals that were originally situated near or at the northern distributional limit of reefs as “subtropical reefs” rather than “marginal reefs”. “Marginal” is being used here in terms of the paleogeographic setting instead (marginal sea vs. open ocean). No valid criterion exists for inferring symbiosis with zooxanthellae in scleractinian corals from skeletal architecture (Perrin and Bosellini, 2012; Rosen, 2000; Stanley Jr and van de Schootbrugge, 2018; Wilson and Rosen, 1998); the terms “reef coral” or “z-coral” are used here under the assumption of extant and extinct generic taxa forming reefal frameworks in shallow water to have been zooxanthellate in the past as well.

2.2. Materials

The fossil z-corals (n = 74) presented herein were collected according to the criterion of excellent preservation of both the original skeletal structures and primary porosity as a prerequisite for measurements of stable isotope proxies and skeletal calcification variables. The coral fossils were collected from as many sites and discrete time-slices of the late Cenozoic as possible, in order to get a complete picture of z-coral growth environments. The sampling localities in Europe, North America, and the Caribbean cover tropical and subtropical settings within and outside the reef window, and were classified coral reef, or level-bottom coral community (Fig. 2). However, most of the sites were close to shore (< 15 km of distance) and do not fit the reef growth window proper. In order to identify possible hinterland effects in the isotope and growth data, growth environments were categorized according to field evidence or literature information as “open ocean”, “marginal sea”, “clear water”, “turbid”, “elevated salinity”, “deep”, “seep” and “upwelling” in addition to “tropical” and “subtropical” (Table 1). The fossil dataset represents 16 geological time-slices being between 20.8 and 1.2 Ma old. It allows describing coral calcification patterns during the period of (1) the late stage of the transition from greenhouse to icehouse in the late Oligocene to middle Miocene (before ca 17 Ma), (2) the MMCO (ca 17 to 15 Ma) and Middle Miocene Climatic Transition (MMCT, ca 15 to 13 Ma) with the middle Badenian Salinity Crisis of the Central Paratethys (MBSC, 13.8 Ma), (3) the beginning of the Northern Hemisphere Glaciation during the late Miocene and onset of the Messinian Salinity Crisis of the Mediterranean (MSC, 5.6 Ma), and (4) the intensification of the Northern Hemisphere (NH) glaciation after 2.9 Ma (Fig. 2, Table 1). The majority of specimens belongs to the genera *Porites* (n = 34), *Solenastrea* (n = 21), *Tarbellastraea* (n = 9) and *Orbicella* (n = 5), whereas the genera *Stephanocoenia* (n = 2), *Goniopora* (n = 1), *Siderastrea* (n = 1), and *Favites* (n = 1) are of minor importance. Details regarding the taxa, location, paleogeographic setting together with information on the growth environment and geological age are summarized in Fig. 2 and Tables 1 and S1. Photographs and X-radiographs of representative specimens from each time-slice can be found in the electronic supplement (color plates S1 – S16).

2.3. Methods

The preservation state of the coral specimens was investigated using a suite of visual (including petrography and SEM), mineralogical (XRD and Raman microspectrometry, the latter performed on thin-sections in some specimens only), oxygen and carbon stable isotope analyses ($\delta^{13}C$, $\delta^{18}O$) and X-radiography. For the published specimens, analytical and screening methods can be found in the cited publications (Table 1). Most diagenetic alterations are visible in hand specimens, thin-sections, or X-ray photographs (Plate 1/A–H).

2.3.1. X-ray diffraction (XRD)

In order to detect the presence of finely disseminated contaminations by calcite formed during freshwater or burial diagenesis (Plate 2/H, I), we performed X-ray diffraction analyses (XRD) of powder samples (250 mg) drilled from coral slices. For XRD, we used a Rigaku Miniflex diffractometer with scanning angles of 20° to 60° 2θ. The detection limit of the method is ~1 %.

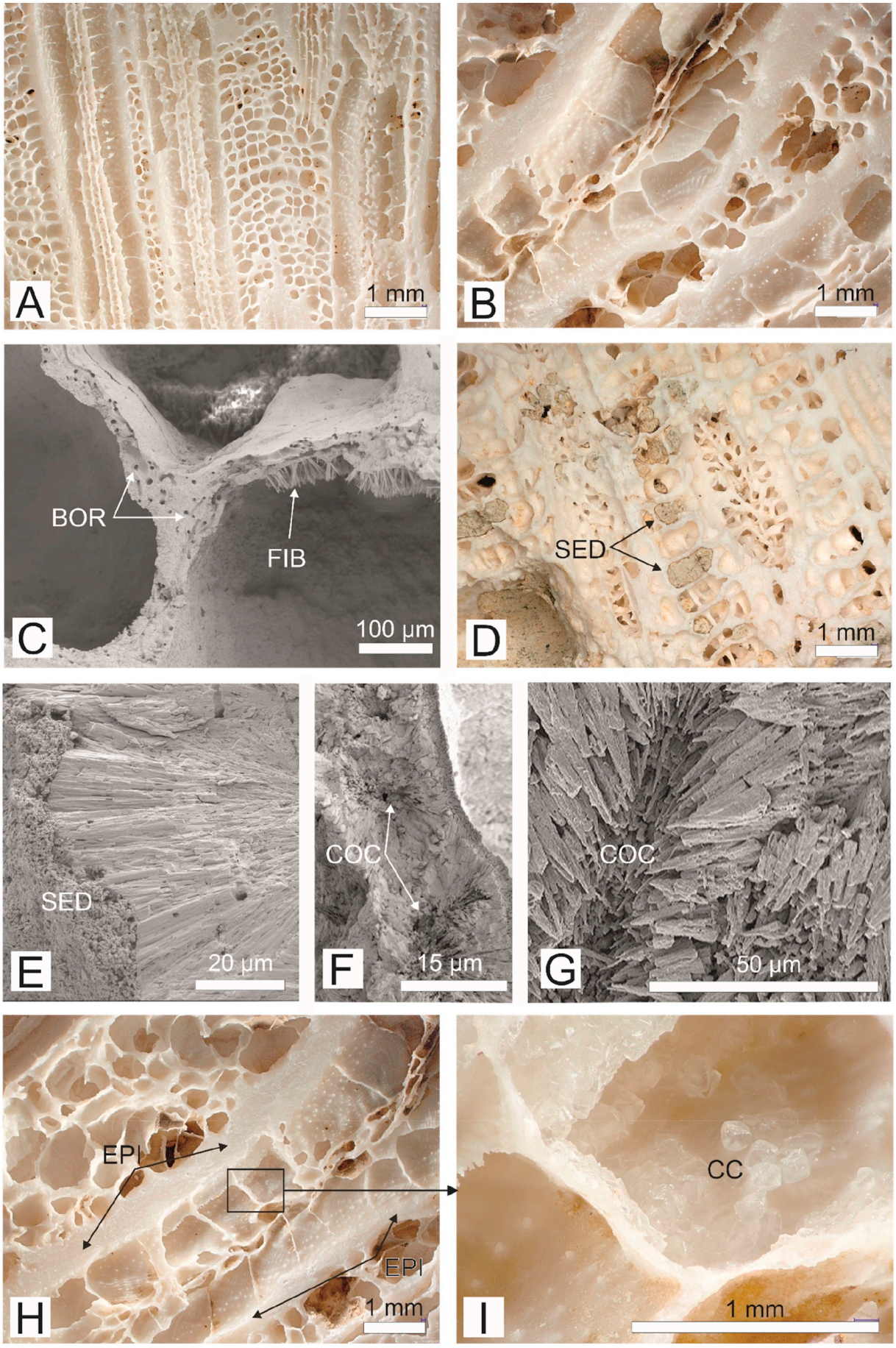

(caption on next page)

Plate 2. Preservation of z-corals.

Figure A. Overview of a longitudinal section showing corallite and bulbous coenchyme. Skeletal surfaces show all anatomical detail. Skeletal structures do not show any evidence of dissolution; skeletal porosity is pristine and not modified by cementation. Polished slab (*Orbicella*, 463K2S1, Late Miocene, Dominican Republic).

Figure B. Overview of a corallum showing two corallites and bulbous coenchyme. Skeletal surfaces show all anatomical detail. Skeletal structures do not show any evidence of dissolution; skeletal porosity is pristine and not modified by cementation. Polished slab (*Orbicella*, 465AS2, Late Miocene, Dominican Republic).

Figure C. Patch of marine needle cement (FIB) partially infilling primary skeletal porosity. The skeleton is densely perforated by microborings (BOR); the microborings are open and not filled with secondary carbonate. These two types of marine alteration are inherent to z-corals of all ages, including the recent, and do not forbid comparisons to be made between fossil and recent corals. SEM photograph (EP9C, Plio-Pleistocene, Florida).

Figure D. Oblique section of a corallum. Some of the original primary skeletal porosity is filled with marine sediment (SED), a feature common to fossil and recent corals. Polished slab (*Solenastrea*, 465BS2, Late Miocene, Dominican Republic).

Figure E. SEM view of fracture surface showing radial arrangement of crystal fibers perforated by some microborings. Primary skeletal porosity is partially infilled with marine sediment (SED). Marine sediment infilling skeletal pores was removed from the skeletons prior to further analyses, if possible (EP9d, Plio-Pleistocene, Florida).

Figure F. Fracture surface showing radial arrangement of crystal fibers and some dissolution at the centers of calcification (COC). SEM photograph (*Orbicella*, EP2, Plio-Pleistocene, Florida).

Figure G. SEM view of a specimen showing dissolution enlarged COCs and contacts between radial cristallites causing a chalky condition of the skeleton. If not patchy, skeletons showing this type of preservation were not used for density measurements (*Tarbellastrea*, MG9, Late Miocene, Crete).

Figure H. Longitudinal section (polished surface) showing corallite with thick epitheca (EPI) surrounded by coenchyme. Skeletal surfaces and most of the skeletal porosity are in pristine condition. Polished slab (*Orbicella*, 465AS2, Late Miocene, Dominican Republic).

Figure I. Detail from 8 shows patch of rhombohedral calcites (CC) between dissepiments of an otherwise pristine corallite. This type of cementation poses no problem to proxy analysis, because all carbonate (septa, dissepiments) within the thecae (EPI in H) was mechanically removed prior to drilling it for powder samples. Polished slab (*Orbicella*, 465AS2, Late Miocene, Dominican Republic).

2.3.2. Raman microspectrometry

Raman microspectrometry provides qualitative analyses with a spatial resolution of 1-2 micrometers and was used to obtain complementary mineralogical information on some coral specimens from Aquitaine (Saint-Martin d´Oney, site 1, Table 1). Analyses were performed directly on uncovered thin sections using a Jobin Yvon Horiba HR800 LabRam® spectrometer operating with a green 514.732 nm exciting line and with a spectral window of 130-1600 cm^{-1}. The system includes an optical microscope and a video camera allowing the analytical spot to be precisely positioned.

2.3.3. Oxygen and carbon stable isotopes

Consecutive samples for stable isotope analysis were taken along transects on single corallites (DeLong, 2015). Prior to sampling specimens with large corallites (e.g. *Orbicella*), all internal structures of one selected corallite were mechanically removed using a handheld microdrill in order to ensure selective sampling of the wall portion of the skeleton and to exclude effects related to materials derived from corallite internal skeletal elements or contaminations from secondary carbonate cement (aragonite or calcite) on measured isotope ratios (Leder et al., 1996). This procedure was not applied to *Porites*, because the skeletal architecture and small size of the corallites precludes any attempt to sample specific portions of the corallites. For this reason, we only sampled specimens of *Porites* that did not show significant amounts of marine aragonite cements. Specimens displaying microscopic, X-radiographic (dark spots in X-radiographs) or XRD (> 1 % of calcite) evidence for the presence of calcite were not used for stable isotope analysis. Sample powders were taken using a microdrill fixed to a manually-operated XYZ stage for drilling sample powders at constant step distances of 0.5 or 0.7 mm. A drill bit with a diameter of 0.6 or 0.8 mm combined with a drilling depth of 0.5 mm yielded > 40 µg of sample powder which was the minimum amount of powder needed for a single analysis. Mean values for a given specimen were determined as the arithmetic mean of all individual measurements, or from homogenized milling powder. Oxygen and carbon stable isotope ratios were measured at the Institute of Geophysics and Geology, Leipzig University (Germany). Carbonate powders were reacted with 105 % phosphoric acid at 70 °C using a Kiel IV online carbonate preparation line connected to a MAT 253 isotope ratio mass spectrometer. All carbonate values are reported in per mil (‰) relative to the V-PDB standard. Reproductibility was monitored by replicate analysis of laboratory standards and was better than ± 0.04 ‰ (1σ) for $\delta^{13}C$ and better than ± 0.06 ‰ (1σ) for $\delta^{18}O$.

For the internal age model of the coral records, we used density bands visible on X-ray photos and / or cyclic variations of the $\delta^{18}O$ values and assumed they reflect seasonal variations of ambient water temperature (Plate S10-S16). The beginning of each individual isotope year was identified as the most positive $\delta^{18}O$ value ("winter") of a $\delta^{18}O$ cycle. Within one year, extension rate was assumed to be constant and internal chronologies established by linear interpolation. Based on a

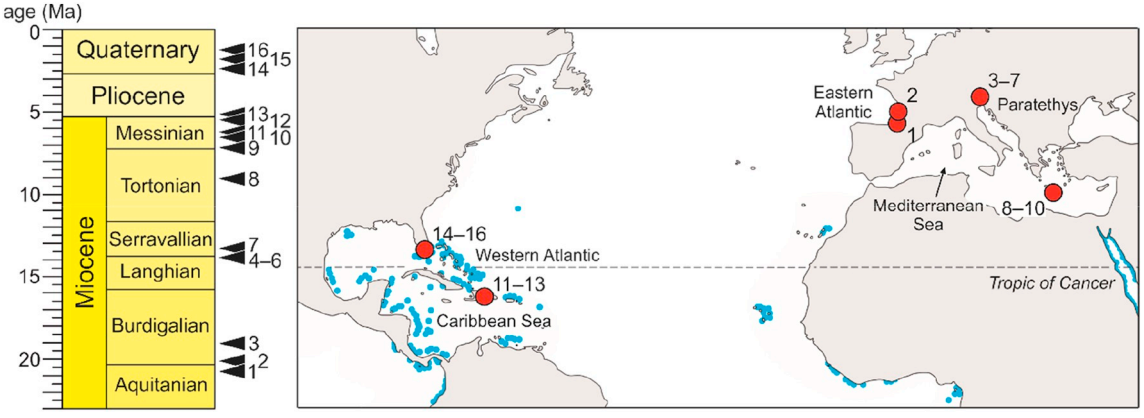

Fig. 2. Stratigraphic and geographic distribution of the sampling sites (numbers refer to Table 1) and modern reefs (blue). Chronostratigraphy according to Gradstein et al., 2012), recent reefs from Veron (2000).

Table 1
Sampling sites and categorization of growth environments. UL = Leipzig University, Germany.

#	Site	Region	Paleogeographic setting	Shallow-water environment	Stage, tuned age	References
1	Saint-Martin d´Oney (France), Coll. Perrin (n = 3)	Eastern Atlantic (Aquitaine Basin)	Subtropical reef, open high-energy shelf	Siliciclastic shelf, sandy shoreface (clear water), non-framework coral community	Aquitanian, 20.8 Ma (21.0-20.4 Ma)	Lozouet et al. (2001); Perrin and Bosellini, (2012). Sr-ages from Perrin & Lozouet PICS4723 (unpubl.)
2	Bordeaux region (Pessac, Merignac, Péloua, France), Coll. Corrège and Coll. Réserve Naturelle géologique de Saucats-La Brède (*n* =8)	Eastern Atlantic (Aquitaine Basin)	Subtropical reef, open high-energy shelf	Siliciclastic shelf, clear water, coral patches	Burdigalian, 20.3 Ma (generalized age)	Cahuzac and Chaix, (1996); Cahuzac et al. (1997); Meulenkamp et al. (2000); Parize et al. (2008); Popov et al. (2004)
3	Eggenburg (Austria), Coll. Felix UL (n = 1)	Paratethys (Vienna Basin)	Subtropical reef, marginal basin	Siliciclastic ramp, turbid, patch reef or non-framework coral community	Burdigalian, 19.2 Ma	Popov et al. (2004), Harzhauser, pers. comm. 2019.
4	Wiesfleck (Austria), UL collection (n = 1)	Paratethys (Styrian Basin)	Subtropical reef, marginal basin	Siliciclastic ramp, turbid, non-framework coral community	Langhian, 14.0 Ma	Popov et al. (2004), Harzhauser, pers. comm. 2019.
5	Nussdorf (Austria), Coll. Felix UL, (n = 1)	Paratethys (Vienna Basin)	Subtropical reef, marginal basin	Siliciclastic ramp, turbid, semi-restricted, non-framework coral community	Langhian, 14.0 Ma	Harzhauser et al. (2014); Popov et al. (2004), Harzhauser, pers. comm. 2019.
6	Drasenhofen (Austria), UL collection (n = 1)	Paratethys (Vienna Basin)	Subtropical reef, marginal basin	Siliciclastic ramp, turbid, non-framework coral community	Langhian, 14.0 Ma	Harzhauser et al. (2014); Popov et al. (2004), Harzhauser, pers. comm. 2019.
7	Pötzleinsdorf (Austria), UL collection (n = 1)	Paratethys (Vienna Basin)	Subtropical reef, marginal basin	Siliciclastic ramp, turbid, non-framework coral community	Serravallian, 13.4 Ma	Harzhauser et al. (2014); Popov et al. (2004), Harzhauser, pers. comm. 2019.
8	Psalidha (Crete, Greece), UL collection (*n* = 13)	Eastern Mediterranean (Messara Basin)	Subtropical reef, marginal basin	Clastic ramp, turbid, patch reef	Early Tortonian, 9.0 Ma	Brachert et al. (2006a); Mertz-Kraus et al. (2009a); Mertz-Kraus et al. (2008); Mertz-Kraus et al. (2009b)
9	Pig Farm, Moni Gorgolaini (Crete, Greece), UL collection (n = 1)	Eastern Mediterranean (Iraklion Basin)	Subtropical reef, marginal basin (semi-restricted)	Clastic ramp, turbid, patch reef or non-framework coral community	Early Messinian, 7.1 Ma	Mertz-Kraus et al. (2009a); Mertz-Kraus et al. (2008); Mertz-Kraus et al. (2009b)
10	Road section, Moni Gorgolaini (Crete, Greece), UL collection (*n* = 4)	Eastern Mediterranean (Iraklion Basin)	Subtropical reef, marginal basin (semi-restricted)	Carbonate bank, clear-water, semi-restricted patch reef	Early Messinian, 6.5 Ma	Brachert et al. (2006a); Brachert et al. (2007); Mertz-Kraus et al. (2009a); Mertz-Kraus et al. (2008); Mertz-Kraus et al. (2009b)
11 – 13	Dominican Republic, UL collection, n = 4 *n* = 3 n = 3	Caribbean (Cibao Basin)	Tropical, open shelf / marginal basin,	Siliciclastic shelf, turbid water, non-framework coral communities and patch reefs	Messinian / Zanclean, 6.2 Ma 5.5 Ma 5.2 Ma	Denniston et al. (2008); Weiss et al. (2017)
14 – 16	Southern Florida, USA, UL collection *n* = 7 n = 8 n = 4	Western Atlantic (Florida Platform)	Subtropical reef, attached platform	Carbonate platform, clear-water and turbid settings, variable upwelling, non-framework coral communities and reefs	Pleistocene, 2.5 Ma 1.8 Ma 1.2 Ma	Böcker, (2014); Brachert et al. (2016a); Brachert et al. (2016b); Roulier and Quinn, (1995)

constant sampling distance of 0.5 mm (0.7 mm), annual extension rates were inferred from the number of isotope samples between two winter values.

For any given time-slice (Table 1), the coral stable isotope values were corrected for global seawater effects using the smoothed version (5-point running average) of the "Zachos curve" (Zachos et al., 2001). We first calculated the difference between the present-day and past deep-sea value for a given time-slice (e.g. for oxygen: $\Delta\delta^{18}O_{deep} = \delta^{18}O_{deep\ recent} - \delta^{18}O_{deep\ geol}$) and added it to the measured coral isotope value $\delta^{18}O_{coral}$ of that time-slice ($\delta^{18}O_{coral\ calib} = \delta^{18}O_{coral} + \Delta\delta^{18}O_{deep}$). The same was done for $\delta^{13}C$. This re-calibration does not take into account bottom water temperature effects on $\delta^{18}O_{carbonate}$ (Lear et al., 2015) and spatial heterogeneity of surface water $\delta^{18}O$ (LeGrande and Schmidt, 2006). To account for extension-rate-related kinetic isotope effects, $\delta^{18}O_{coral\ calib}$ values were also transformed to a theoretical mean coral $\delta^{18}O_{theor}$ value at a common mean extension rate of 1.0 cm yr^{-1} following the procedure described by Felis et al. (2003). No such correction is available for $\delta^{13}C$ although analogous effects have been reported (McConnaughey, 1989). Coral sampling sites were dated by combined biostratigraphic data and Sr-isotope ages and then tuned to the closest global $\delta^{18}O_{deep}$-minimum (= highstand of sea-level) of the Zachos curve, if no other field-evidence for sequence-stratigraphic position was available ("tuned age" in Table 1). For the corals from the Bordeaux region (Table 1), we give a generalized age, since detailed age relationships between sites are not fully clear yet.

2.3.4. X-radiography

Coral slabs were X-rayed with a digital X-ray cabinet (SHR 50 V). Density measurements were made using X-ray densitometry based on CoralXDS software (freeware) (Helmle et al., 2002). This method relies on the gray values recorded by X-radiographs from coral slabs (Plate S10-S16). Gray-scale calibration of X-radiographs (digital) to skeletal density is achieved by a process using X-radiographs from an aluminum wedge and aluminum plates having the same thickness as the coral slices for a background picture. Calibrations were checked and iteratively improved by measuring transects crossing the empty screen of the X-ray cabinet and a coplanar slice of massive aragonite having the same thickness as the coral slab to be measured (Fig. 3). Calibration standards were produced from micritic masses of Karlovy Vary travertine (Czech Republic) or shells of the large bivalves *Tridacna* and *Glycymeris*. This procedure allowed for a precise calibration of grey value between zero density (empty screen) and 2.93 g cm^{-3} density of massive aragonite (region of interest of Fig. 3). Densitometry of corals was performed along transects parallel to the corallites and the width selected according to the diameter of the corallites. Transects were positioned so as not to include macroscopic borings or otherwise altered portions of the skeleton. Mean skeletal density was calculated as the mean of all individual measurements along a given transect. A more detailed description of the method has been presented previously (Brachert et al., 2016a, 2016b). Calcification rate (g cm^{-2} yr^{-1}) was determined as the product of annual extension rate (cm yr^{-1}) and skeletal bulk density (g cm^{-3}) (Lough and Barnes, 2000). The term "calcification rate" is used here in a broadened way for "net calcification rate", as it also includes effects of microendolithic infestation and marine cementation on bulk density. The latter are, however, inherent to the recent calibration datasets as well.

2.3.5. Statistics

Statistical analyses were performed using the free software package Past (version 3.25). We used linear bivariate statistics to test for significant correlations between variables indicated by the coefficient of determination (R^2) and the p-value < 0.05. Environmental effects on extension rate, skeletal bulk density, and calcification rate were assessed by two-sample t-tests assuming equal mean values after checking for normal distribution.

2.4. The Recent reference and validation datasets

For a detailed evaluation of the calcification trends of z-corals from the late Cenozoic to the present-day, we use a reference dataset for the recent Indo-Pacific (IP) that we test with an independent validation dataset from the Western Atlantic-Caribbean (WA-C). In order to account for the heterogeneous dataset available from the Neogene and Quaternary, the reference and validation datasets were constructed so as to rely on separate biogeographic regions (IP vs. WA-C), different taxa of massive z-corals (*Porites* vs. *Orbicella*), and a set of distinct growth environments inside and outside the reef growth window as categorized in Table 1.

The reference dataset is from data on the recent massive coral *Porites* spp. (with few data from *Pavona* and *Platygyra*) from the IP. It is an extension of the classical dataset for the Great Barrier Reef (GBR) region (Lough and Barnes, 2000) through additional literature data from a variety of environments inside and outside the reef-window. It includes information from the tropics to the subtropical outposts of the global reef belt, from very shallow to deep (> 20 m) reef settings, from clear to turbid waters, semi-restricted (elevated salinity) vs. open-ocean environments, as well as from upwelling zones and volcanic CO_2 vents. This classification was kept as simple as possible in order to allow its use for fossil and recent corals in a compatible way (Table 1). In many cases, the sites of coral growth were classified into more than one category. Some factors known to have negative effects on coral growth (e.g. exposure to waves and storms) have not been included in the classification, because the information supplied on those factors in the literature is sparse, or even not available for fossil corals.

The validation dataset was constructed in an analogous way, from literature data on massive corals of the recent WA-C. This dataset also includes corals from a multitude of environments that were categorized as for the IP. In contrast to the reference dataset, it contains essentially data from *Orbicella* (in addition to *Porites astreoides* and *Diploria*). For every site of coral growth, IP and WA-C, literature data were averaged if measurements from more than one coral were available from one site to keep data consistent with the Lough and Barnes dataset (Lough and Barnes, 2000).

3. Results and discussion

3.1. State of preservation of the coral specimens: significance for proxy and calcification records

Specimens selected for bulk density and proxy measurements during this study display clean skeletal surfaces and all original skeletal microstructural details typical of the corresponding taxa (Plate 2/A, B, Plates S1 – S9). Hence, the specimens lack voluminous infillings of intraskeletal porosity with marine sediment, isopachous fringes of acicular marine cements except for some small patches of secondary overgrowths of fibrous marine or blocky freshwater cement (Fig. 1/B, Plate 2/C, D, E, I). Fracture surfaces of the skeletons show the regular, radial arrangements of aragonite fibers more or less affected by macroscopic and microendolithic borings (Plate 2/C, E). The microborings do not show any secondary infills. While macroscopic borings were easily identified on X-radiographs and discarded during density measurements, density measurements integrated over microborings because they are invisible in X-radiographs. Nonetheless, microborings and cements occur also everywhere in recent reef corals and their effects are inherent to reference data of bulk density as well.

Diagenetic alteration is typically patchy and causes domains of pristine and variably altered skeleton to co-exist at small spatial scales (Griffiths et al., 2013; McGregor and Gagan, 2003; Mertz-Kraus et al., 2009b) (Plate 1/C-F). Dissolution of skeletal aragonite starts at a very early stage and affects primarily the centers of calcification (COC) (Perrin and Cuif, 2001), termed also rapid accretion deposits or early mineralization zone within thickening deposits (Cuif and Dauphin,

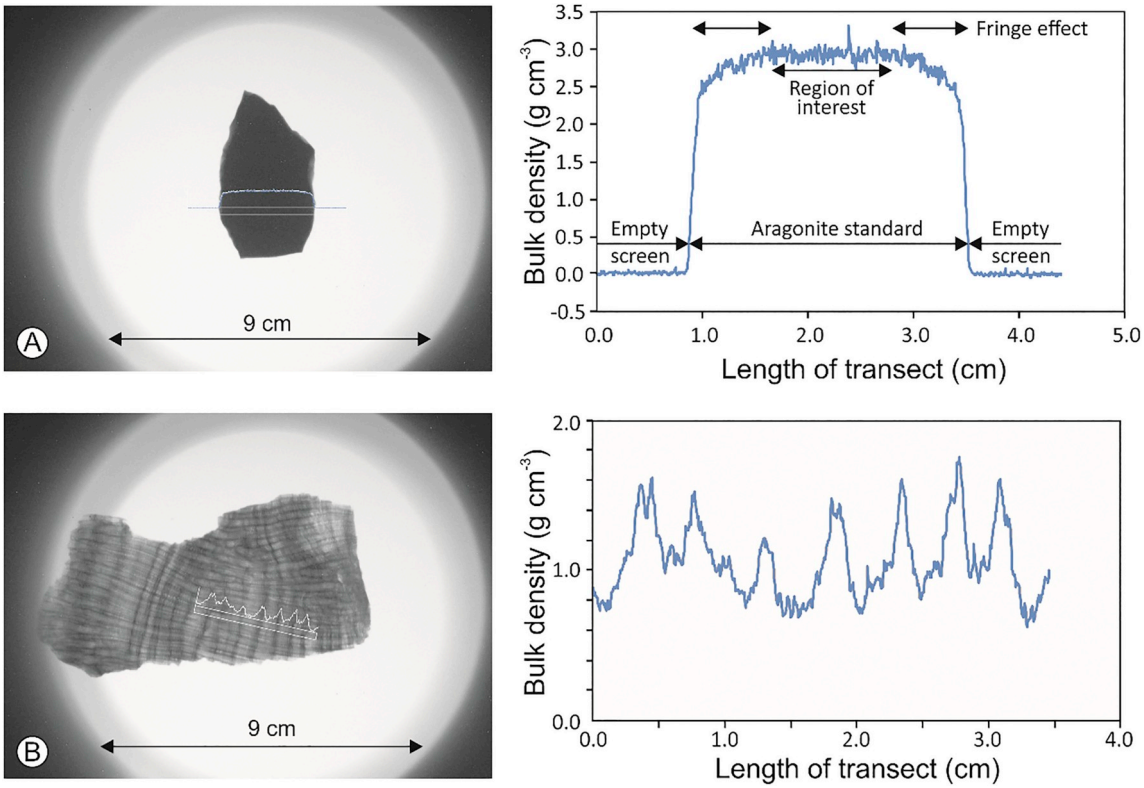

Fig. 3. Method of bulk density measurement. Density measurements rely on gray-scale analyses of calibrated, digital X-ray photos. A: Testing of calibrations. X-radiograph of standard material showing a measurement transect that stretches from the empty screen over the standard and empty screen again. According to the calibration used, density is 0.01 ± 0.02 g cm^{-3} for the empty screen and 2.93 ± 0.07 g cm^{-3} for the massive aragonite slab (region of interest). B: Measurement of bulk density from a coral (*Solenastrea*, 465 B S2). Transects were positioned within the center of the screen only; long records were combined from several consecutive transects.

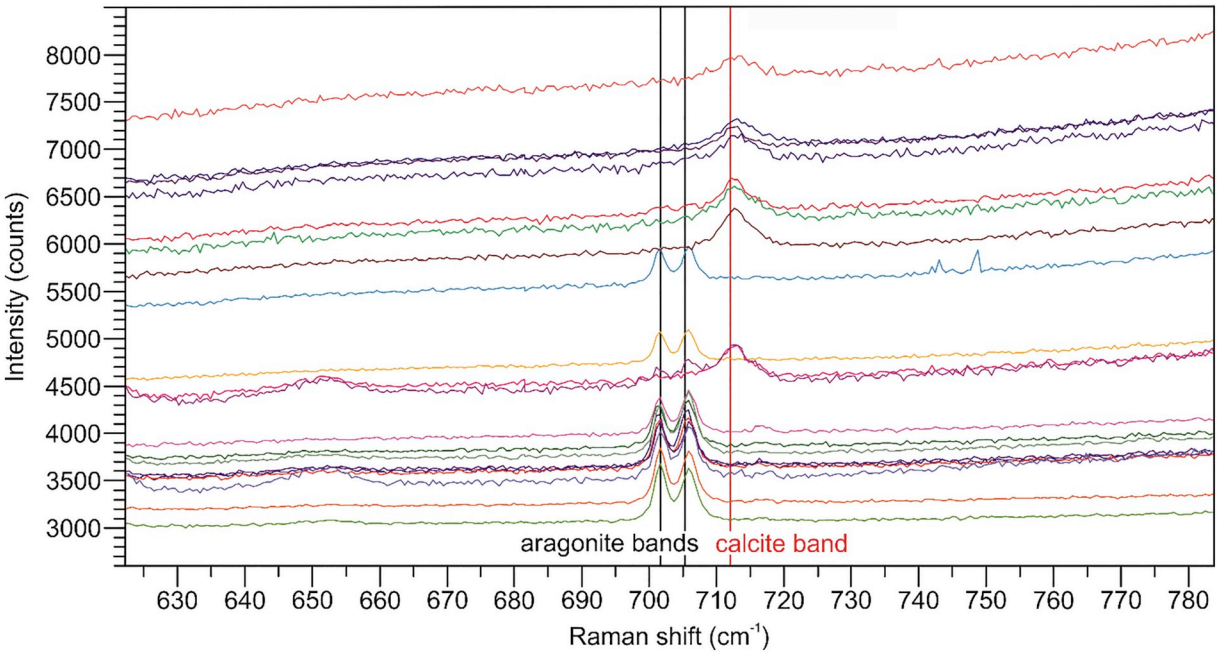

Fig. 4. Coral diagenesis, Raman spectra obtained in an early Miocene *Porites* specimen from Aquitaine (site 1, Saint-Martin d´Oney, France). Spectra are shown in the 700 cm^{-1} region where discrimination between aragonite and calcite is straightforward. Aragonite is characterized by the doublet at 701-706 cm^{-1} while calcite shows a single band at 712 cm^{-1}. In some spectra, only aragonite is detected, while some others display only calcite.

2005; Stolarski, 2003) (Fig. 1/C, Plate 2/F). With increasing intensity, dissolution causes widening of the COCs, finally forming an interconnected system of hollow skeletal structures before complete destruction of the skeleton (Reuter et al., 2005) (Fig. 1/D, Plate 2/G). Continued dissolution of the skeleton may also follow the contacts of the fibers and cause the formation of a chalky condition (Plate 2/G). Although these two forms of leached preservation have no negative effect on stable isotope proxies (Mertz-Kraus et al., 2008), they cause reductions of skeletal bulk density. Skeletons showing this intense dissolution were not included in the measurements of this study, except when the occurrence of the feature was patchy and could be avoided during measurements. Some dissolved COCs display partial infillings of calcite cement that compensates for skeletal losses. Such a diagenetic feature is easily identified from observation of thin sections at high magnification in optical microscopy. The calcitic mineralogy of cement filling the dissolved COCs is clearly evidenced from Raman spectra (Fig. 4). This rare type of preservation poses no significant problem for measurements of bulk density, because it affects only a very small proportion of the total skeleton, and the density of calcite (2.71 g cm^{-3}) is not too different from that of aragonite (2.93 g cm^{-3}).

The presence of cements infilling primary skeletal porosity causes an increase in bulk density and modifications of proxy data. With regard to marine aragonite cement (Plate 2/C), this is a problem inherent to recent corals as well and poses no problem for a comparative analysis between fossil and recent corals. In contrast, freshwater (or burial diagenesis) calcite cement is, if present, specific to fossil corals and may partially to fully seal skeletal pores (Frankowiak et al., 2016; Griffiths et al., 2013) (Fig. 1/C, E, F, Plate 2/C–H). As a result, the analysis of skeletal bulk density and isotope proxies is rendered impossible for this type of preservation, and specimens showing this condition were not used for proxy analysis and density measurement. With respect to isotope analysis, this is not true for very patchy occurrences of cement and coral taxa with large corallites, because the surfaces of the thecae were cleaned mechanically prior to sampling them for proxy analyses (Plate 2/I). The sparry calcite mosaics replacing the skeletons of most fossil corals in reefal limestone often displays ghost structures of the original annual growth bands. Hence, extension rate can be measured even with fully altered skeletons (Reuter et al., 2005) (Plate 1/1-2).

3.2. Stable isotope data

The mean $\delta^{13}C$ and $\delta^{18}O$ values of all individual corals range from -3.35 to 0.31 ‰ and -4.16 to -2.24 ‰ with a total mean of -1.40 ± 1.00 ‰ and -3.12 ± 0.52 ‰, respectively (Tab. S1). While the mean $\delta^{13}C$ values are fully within the range of values of present-day reef corals, many of the mean $\delta^{18}O$ values are more positive than "typical" for the reef window and more consistent with asymbiotic corals (Frankowiak et al., 2016; Stanley and Swart, 1995) (Fig. 5). For a semi-quantitative understanding of the mean coral isotope data, we removed the global, temporal trends from the individual coral records and extension rate effects on $\delta^{18}O$. In a scatter plot of $\delta^{13}C$ and $\delta^{18}O$, the recalibrated means of each coral specimen ($\delta^{13}C_{coral\ calib}$, $\delta^{18}O_{coral\ calib}$) are consistent with recent reef coral $\delta^{13}C$, while the majority of the mean $\delta^{18}O_{coral\ calib}$ values is even more positive than the uncorrected values and less consistent with modern values when only global seawater effects are taken into account (Frankowiak et al., 2016; Swart, 1983) (Fig. 5/B). Values of $\delta^{18}O_{coral\ calib}$ being further re-adjusted for a common extension rate of 1 cm yr^{-1} ($\delta^{18}O_{theor}$) are more negative, albeit not all of them are fully consistent with "typical" modern z-coral values of the reef window (Felis et al., 2003) (Fig. 5/C). Additional information on the subject can be found in chapter 3.2.1 (Significance of sclerochronologies). The result of the recalibrations does not imply, however, that some of the fossil corals were asymbiotic, because paired $\delta^{13}C_{coral\ calib}$ and $\delta^{18}O_{coral\ calib}$ do not show the positive correlation typical of asymbiotic corals, and all of our data are from known symbiotic taxa. In this respect, it should be noted that an asymbiotic

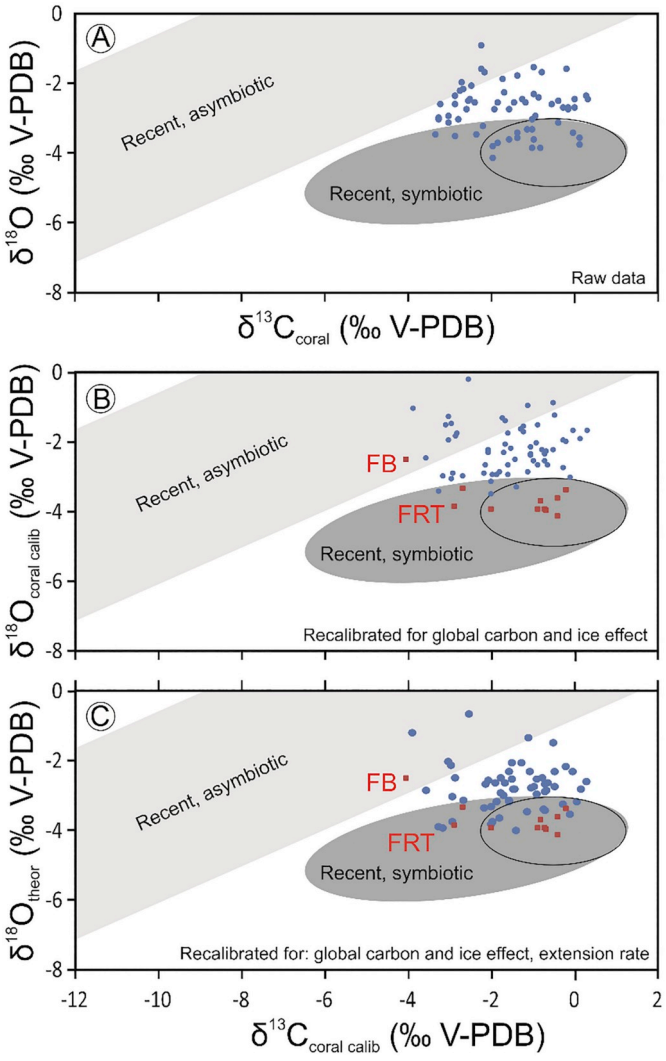

Fig. 5. Mean oxygen and carbon stable isotope values ($\delta^{18}O$, $\delta^{13}C$) of fossil symbiotic corals (z-corals) compared to recent symbiotic and asymbiotic corals (modified from Frankowiak et al., 2016). Upper panel: raw data (blue dots), middle panel: values recalibrated for global ice and carbon cycle effects (blue dots) (Zachos et al., 2001). Lower panel: values recalibrated for global ice and carbon cycle effects with an additional recalibration of $\delta^{18}O$ values for a common mean extension rate of 1 cm yr^{-1} (blue dots). The small ellipse with black margin delineates the "normal "range of recent z-coral data, complemented by data from Florida Reef Tract (FRT, red squares) and Florida Bay (FB, red square) (Stanley and Swart, 1995). The dark gray ellipse summarizes the range of data for a set of various symbiotic taxa and growth forms from mostly undisturbed reef settings, the light gray field illustrates data from asymbiotic corals (Frankowiak et al., 2016).

signature is also present in a recent z-coral from the semi-restricted Florida Bay (FB) shown here for comparison, whereas $\delta^{18}O$ of corals from the open Florida Reef Tract (FRT) is consistent with a marine, subtropical-reef setting (/B, C).

Over geological time, carbon stable isotope values ($\delta^{13}C_{coral\ calib}$) were normal marine in terms of the recent reef window for most of the time/sites. Negative excursions dated 14.0 Ma and 1.2 Ma were recorded in the Central Paratethys and Florida Platform, respectively (Fig. 6). Both excursions are in the same order of magnitude as covered by the present-day´s FRT - FB gradient and likely reflect similar marine - nearshore gradients (Fig. 6). However, upwelling has been shown to be an equally plausible interpretation for stable isotope signatures of some z-corals from the Florida Platform (Brachert et al., 2016a) (Fig. 6). Recalibrated oxygen isotope values are rather constant over time and

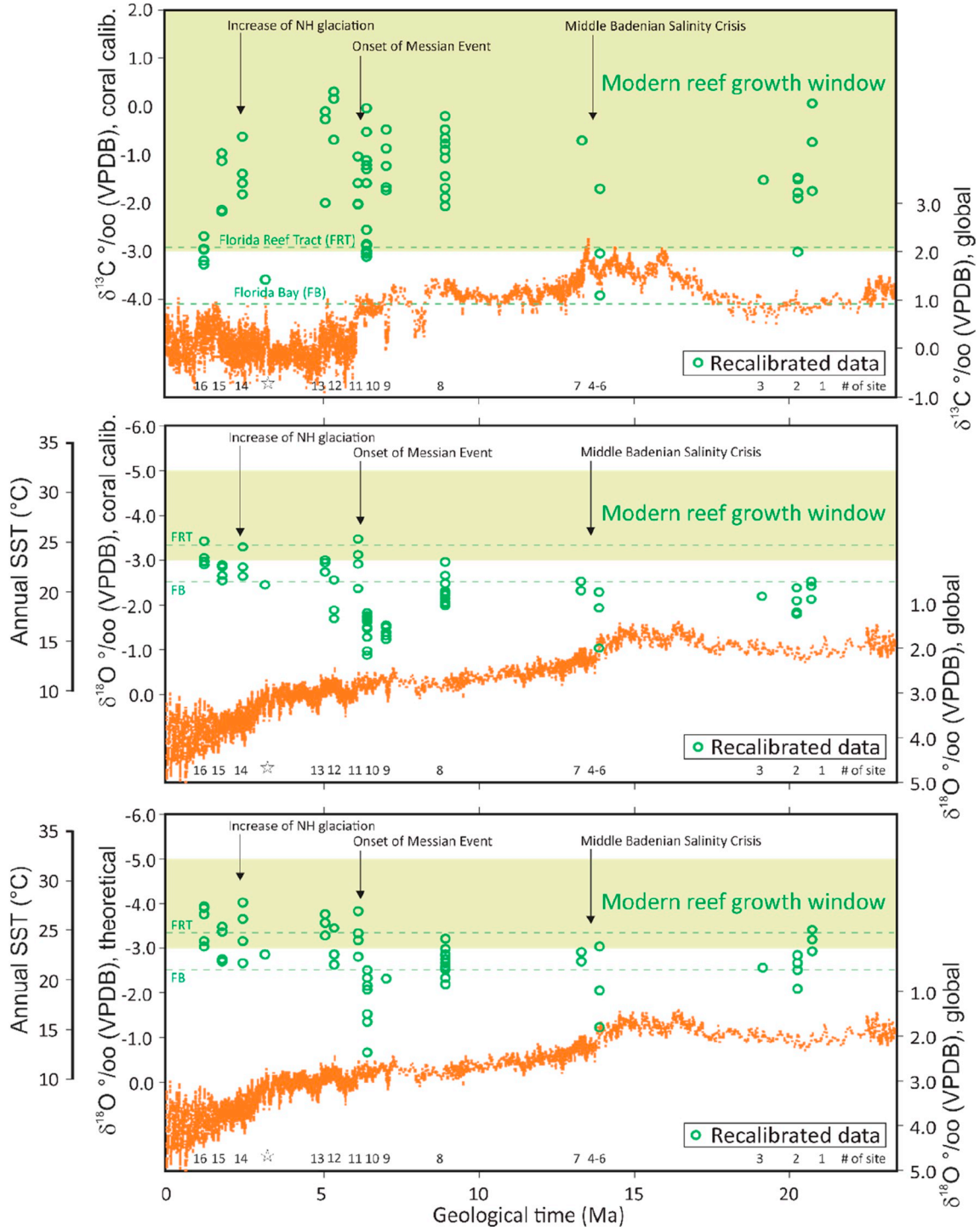

Fig. 6. Recalibrated mean oxygen and carbon stable isotope data from reef corals ($\delta^{13}C_{coral}$, $\delta^{18}O_{coral}$) (green) compared to global trends in deep-sea stable isotope values (orange, 5-point running average, from Zachos et al., 2001). The lower panel shows $\delta^{18}O_{coral}$ corrected for extension rate effects at a common mean extension rate of 1.0 cm yr^{-1} ($\delta^{18}O_{theor}$) according to Felis et al. (2003). The green shade shows stable isotope values of the recent reef window, the dashed green lines give exemplary coral data from Florida Reef Tract (FRT) and Florida Bay (FB) (Brachert et al., 2016a; Stanley and Swart, 1995). Note inverted scale for $\delta^{18}O$ values. Identical scaling for coral and deep-sea data. Annual SSTs according to a calibration for *Orbicella* from Florida Reef Tract and seawater $\delta^{18}O$ = 1.0 ‰ SMOW (Leder et al., 1996). Numbers at the bottom of the diagrams refer to sampling sites as listed in Table 1. Asteriks: data from literature (Roulier and Quinn, 1995). NH = Northern Hemisphere.

range approximately between -4.0 and -2.0 ‰, only interrupted by two positive excursions dated 6.5 Ma and 14.0 Ma (Fig. 6). According to a calibration for *Orbicella* from Florida Reef Tract ($\delta^{18}O_{sea\text{-}water}$ = 1.0 ‰ SMOW, approx. modern Florida seawater) our set of $\delta^{18}O_{coral\ calib}$ is equivalent with mean annual SSTs between 10 and 25 °C (Leder et al., 1996) (Fig. 6). Thus, except for the excursions (Table 1, sites 5, 10), $\delta^{18}O_{coral\ calib}$ = -4 to -2 ‰ is equivalent with a present-day subtropical reef setting, i.e. SSTs near the lower threshold value for reef growth (18°C_{winter}, Table 1, sites 7-9, 14-16) or minimum value for non-framework coral communities (11 – 14 °C_{winter}, Tab. 1, sites 1-7, 9, 11-16) (Veron, 2000) if no significant additional seawater effect through evaporation or large-scale regionality is taken into account (LeGrande

and Schmidt, 2006). This finding agrees well with a position near or beyond the northern margin of the former reef belt for many of the sites (Table 1, Fig. 2).

As a guideline for the further interpretation of the stable isotope data, we use an arid and a seasonally humid subtropical reef setting. A present-day analogue for an arid region is the northernmost Red Sea, allowing for a positive evaporation effect in addition to SST on $\delta^{18}O_{coral}$ (Felis et al., 1998; Heiss, 1994). The assumption of a moderate evaporation effect for the majority of the fossil subtropical reef sites from marginal basins (Table 1, sites 3, 5, 7-13) is supported by $\delta^{13}C_{coral\ calib}$ being fully within the range of recent reef corals from the reef growth window, and $\delta^{13}C_{coral}$ data from the Red Sea in particular. For more humid locations undergoing a rainy period in summer (Table 1, sites 4, 14-16), recent reef corals from southern Florida may serve as an instructive example, because growth data exist for both open-water reefs (FRT) and semi-restricted settings of coral growth (FB). According to the Florida Bay Model (Halley and Roulier, 1999), corals in FB are approximately +1 ‰ in $\delta^{18}O$ more positive due to a net evaporation effect. Hence, with regard to the fossil z-coral sites being from subtropical reef sites (Table 1), mean $\delta^{18}O_{coral}$ values ≥ -1.5 ‰ likely represent the combined effect of low SSTs and various degrees of evaporation. A high degree of evaporation is particularly plausible for the Central Paratethys due to a complex paleogeography and anti-estuarine water exchange with the Proto-Mediterranean (Kováč et al., 2017; Popov et al., 2004) and also for the Mediterranean prior to the Messinian event (Brachert et al., 2007; Sierro et al., 2003). In contrast to the 6.5 Ma $\delta^{18}O$-excursion, that displays normal-marine $\delta^{13}C_{coral\ calib}$ signatures, $\delta^{13}C_{coral\ calib}$ of the 14.0 Ma $\delta^{18}O$-excursion is rather negative, more or less consistent with Florida Bay. This difference in $\delta^{13}C_{coral\ calib}$ between the two sites and excursions reflects the prominent climate with a rainy period during summer in the Central Paratethys region during that time and a rather perennially dry climate in the Mediterranean region, respectively (Bruch et al., 2011; Micheels et al., 2010). The finding of rather positive $\delta^{18}O_{theor}$ signatures for three tropical sites in the Caribbean dated 6.2, 5.5 and 5.2 Ma, is problematic (Table 1, Figs. 2, 6, S1), because the associated muddy clastic lithologies indicate turbid water (Johnson and Pérez, 2006) and apparently seem contradictory with a dry climatic context that would facilitate evaporation and compensate effects of warm SSTs in skeletal $\delta^{18}O$. Nonetheless, marine, reef window-type $\delta^{13}C_{coral\ calib}$ is also in accordance with negligible terrestrial discharge. All in all, the data show that shallow-water reef corals were already perfectly adapted to the oligotrophic reef window by the beginning of the Neogene. Thus, the stable isotope data from the 16 time-slices corrected for global trends provide plausible information on the environments of coral growth and support other evidence for the excellent preservation of the skeletons.

3.2.1. Significance of sclerochronologies

For this assemessment of calcification in scleractinian reef corals over the late Cenozoic, we do not present a review of the $\delta^{18}O$-sclerochronologies available, although significant contributions to paleoclimatology have been made, e.g. by the detection of NAO-type interannual climate variability in the Mediterranean region at 10 Ma (Brachert et al., 2006a). The main limitation for a significant result of a compilation is the very heterogeneous resolution of the individual sclerochronological datasets published. In this contribution, we provide three examples of sclerochronologies and discuss the problem of resolution for coral sclerochronological datasets together with extension rate effects on mean $\delta^{18}O$ values. The examples were selected so that all have approximately the same geological age and represent a subtropical and tropical setting, respectively (Fig. 7, Table 2).

The two sclerochronologies from the subtropics derive from the same geological site but document discrepant seasonal SST contrasts of 6 °C and 9 °C, respectively (Table 2). We ascribe the difference in SST seasonality inferred from $\delta^{18}O$ values to the different annual sampling resolution (samples yr^{-1}) of the two records; datasets with a low number of samples per year (low extension rate; Fig. 7/A, Table 2) underestimate "true" seasonality, whereby no agreement exists in the literature about the resolution required for a reliable documentation of the seasonal SST cycle (Leder et al., 1996; Quinn et al., 1996). An important aspect in this discussion is the type of record, i.e. whether a sclerochronological dataset shows a sinusoidal cycle or a "church window-type" pattern, because the latter is strongly biased to one of the two main seasons. In the subtropical datasets, we document a "church window" pattern (Fig. 7/A, B) which likely reflects that SSTs fell below the closing temperature of calcification during the cool season (Mertz-Kraus et al., 2009a; Mertz-Kraus et al., 2009b). Thus, the cool season is underrepresented in the two sclerochronological records, and the difference in seasonal contrast between the two records is likely an effect of a different discrimination against the winter season by the low and high extension rate record, respectively (Fig. 7/A, B, Table 2). In the tropical sclerochronology presented here, we document a sinusoidal pattern and an even lower seasonality (3 °C) than in both subtropical records, although the resolution of the dataset is very similar to that of the subtropical record with a low resolution (Fig. 7/C, Table 2). Although it is likely that the record underestimates true seasonality, it is plausible that tropical seasonality was only ~50 % from subtropical seasonality documented by the record with a similar resolution. Thus, comparative analyses of sclerochronological data require records of compatible resolution for meaningful results, and care must be taken when interpreted quantitatively. It should be taken into account also, that the resolution of sclerochronological records is not unlimited, but typically limited upward by the number of samples fitting physically into one annual growth increment. Thus, sclerochronologies from z-corals with a low extension rate will have a chronically low resolution by stable isotope values, and new methodological approaches are required to enhance their resolution or establish compatibility of results. A list of Neogene coral sclerochronologies presently available is given in Table 1.

It should be noted, that the two *Porites* shown in Fig. 7/A and B differ in their mean $\delta^{18}O_{coral\ calib}$ values by 0.7 ‰ (equivalent with 3.2 °C annual SST) although they both derive from the same fossil site (Table 2). Thus, it is a fair assumption, that SSTs and seawater values of $\delta^{18}O$ during the growth of the two corals were essentially the same, and differential $\delta^{18}O$ of the two is more likely a reflection of growth-rate-dependent, so-called "vital effects" on isotope ratios (Felis et al., 2003; McConnaughey, 1989). The relationship between annual extension rate and mean $\delta^{18}O_{coral\ calib}$ of the two specimens, complemented by data from other specimens of the same site, is reasonably similar to relevant data from *Porites* of the present-day´s Red Sea (Felis et al., 2003) (Fig. 8). For this reason, we assume that oxygen isotope systematics of the fossil *Porites* from a subtropical site were the same as in the present-day, and applying the correction for growth-rate-effects on $\delta^{18}O$ deduced from the Red Sea corals to the fossil corals as described in this contribution is well justified indeed (Fig. 8).

3.3. Calcification trends

Calcification of the fossil corals is given in terms of three variables: mean annual extension rate, mean skeletal bulk density, and mean annual calcification rate. Mean extension rate ranges from 0.15 to 0.86 cm yr^{-1} (mean: 0.41 ± 0.15 cm yr^{-1}), mean skeletal bulk density from 0.55 to 2.15 g cm^{-3} (mean 1.23 ± 0.37 g cm^{-3}) and mean calcification rate from 0.20 to 1.07 g cm^{-2} yr^{-1} (mean 0.49 ± 0.21 g cm^{-2} yr^{-1}), respectively (Tab. S1). One single specimen shows an exceptionally high extension rate (1.39 cm yr^{-1}) (Fig. 7, 8), but no data for skeletal bulk density and calcification rate are available for this specimen. For this reason, it was not included into the statistical evaluation of calcification variables described below. Over all specimens, the three variables of calcification show highly significant correlations at the level of mean values per specimen (Fig. 9): negative relationships exist between extension rate and skeletal bulk density

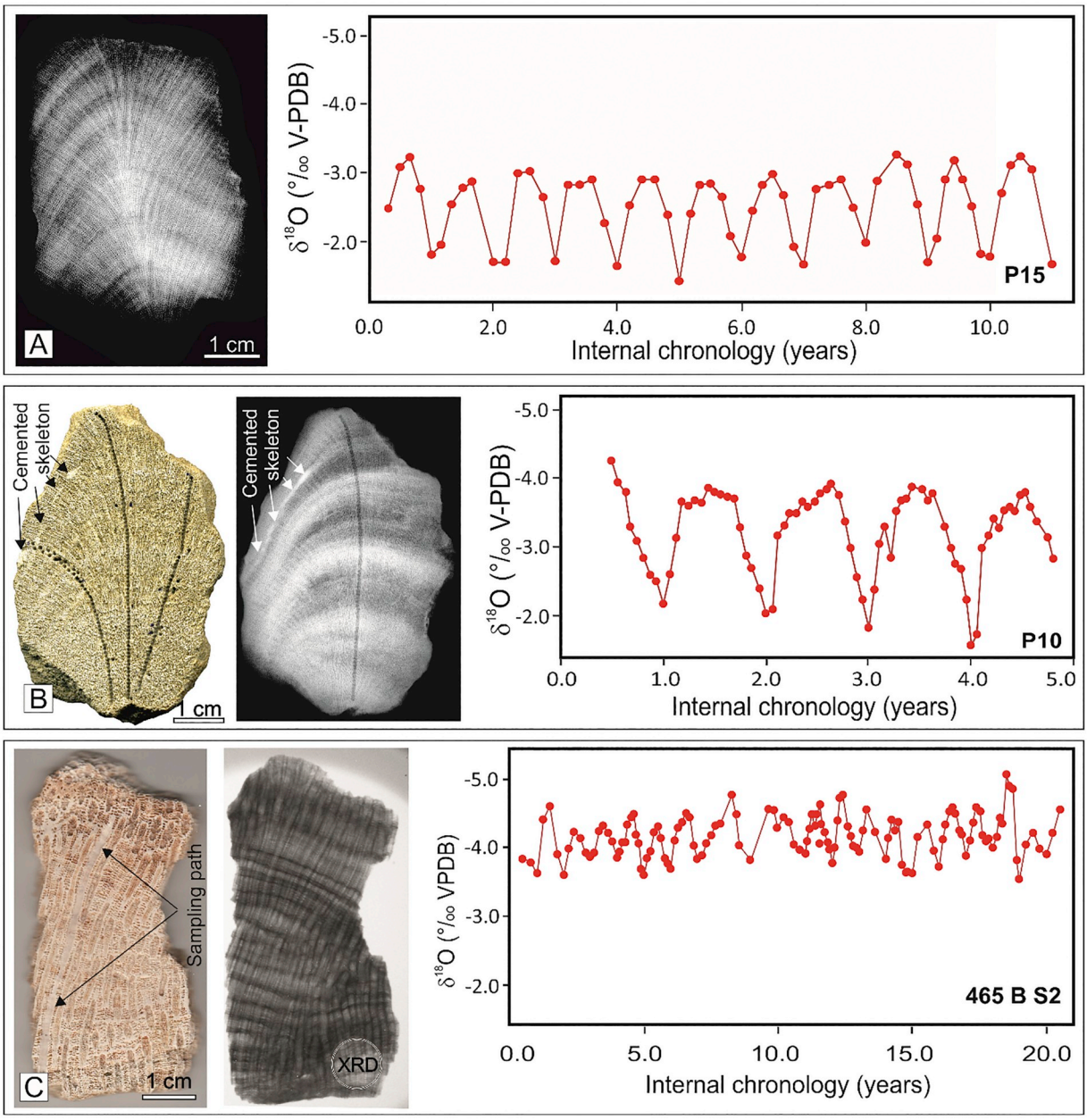

Fig. 7. $\delta^{18}O$ sclerochronologies from a subtropical (A, B) and a tropical (C) reef of late Miocene age. Photographs of coral slabs (reflected light) and X-radiographs (negative prints from X-ray film in A and B, positive print from digital X-ray cabinet in C). A and B: Small massive *Porites* (Ambelouzos Formation, Late Miocene, Psalidha, Crete). Note hole-by-hole sampling tracks following single corallites in (B). Patchy cementatation is well visible in reflected light and X-radiography. Care must be taken not to confuse these thin bands of anomalously high density with "stress bands" (B). C: Fragment of massive *Solenastrea*. The corallite selected for stable isotope sampling was cleared from all corallite internal structures and potential cements prior to sampling of the corallite wall (Upper Cercado Formation, Late Miocene, Arroyo Bellaco, Hispaniola). Light circular patch in in lower right of X-radiograph is from large sample for XRD analysis. Specimen numbers are given on the diagrams and in Table 2.

(R^2 = 0.0931, p = 0.01), and positive relationships exist between extension rate and calcification rate (R^2 = 0.3398, p < 0.001) and calcification rate and skeletal bulk density (R^2 = 0.2955, p < 0.001). With regard to averages per site, however, a significant positive correlation exists only between extension rate and calcification rate (R^2 = 0.4552, p = 0.01) whereas no statistically robust relationships exist between extension rate and bulk density (R^2 = 0.1818, p = 0.11) and bulk density and calcification rate (R^2 = 0.1186, p = 0.28), respectively. Taxonomic or site-specific calcification relationships were not tested because of the small numbers of specimens per taxon and/or site, except for *Porites*, which is the most common taxon in our dataset (46 %). It is indistinguishable from the rest of the specimens and, therefore, we assume there is no taxonomical trend in the available data (Fig. S7). Skeletal bulk density of the fossils is within the range of *Porites* and *Orbicella* from present-day clear-water sites of the IP and WA-C, respectively, whereas the ranges of extension rate and calcification rate are substantially lower and are among the lowest values recorded for z-corals so far (Brachert et al., 2016b; Lough and Barnes, 2000) (Fig. 9).

Very low rates of extension and calcification of the fossil corals is in good agreement with the subtropical positions of most sampling sites (Table 1, Fig. 2), because these two growth variables are essentially driven by water temperature (Lough, 2008; Lough and Barnes, 2000) (Table 1). However, we encountered low rates of extension and

Table 2
Examples of late Miocene coral sclerochronologies. Mean SST contrast was calculated as the mean of the differences between the most positive and negative $\delta^{18}O$ values of a cycle ($\Delta\delta^{18}O$) and using a slope of -0.22 ‰ $\delta^{18}O$ change per degree Celsius (°C) (Druffel, 1997). We also assumed constant sub-annual seawater $\delta^{18}O$. SD: standard deviation.

Setting, geological age (site of Table 1), sample #	Taxon	Mean extension rate (cm yr^{-1})	Mean skeletal bulk density (g cm^{-3})	Mean resolution (samples yr^{-1})	Mean $\delta^{18}O_{coral\ calib}$ ± SD value (‰)	Mean seasonal contrast ($\Delta\delta^{18}O$ ± SD) (‰)	Mean SST contrast (°C ± SD)	Published sclerochronologies
Subtropical, late Miocene, Psalidha, Crete (site 8), P15	*Porites*	0.5	n.a.	5.6	-2.50 ± 0.52	1.3 ± 0.2	5.9 ± 1.0	Brachert et al., 2006b; Mertz-Kraus et al., 2009a; Mertz-Kraus et al., 2008
Subtropical, late Miocene, Psalidha, Crete (site 8), P10	*Porites*	1.4	n.a.	15.9	-3.20 ± 0.60	2.0 ± 0.2	9.1 ± 1.0	
Tropical, late Miocene, Arroyo Bellaco, Hispaniola (site 13), 465B S2	*Orbicella*	0.5	1.16	6.7	-4.16 ± 0.31	0.7 ± 0.3	3.2 ± 1.4	Denniston et al., 2008; Weiss et al., 2017

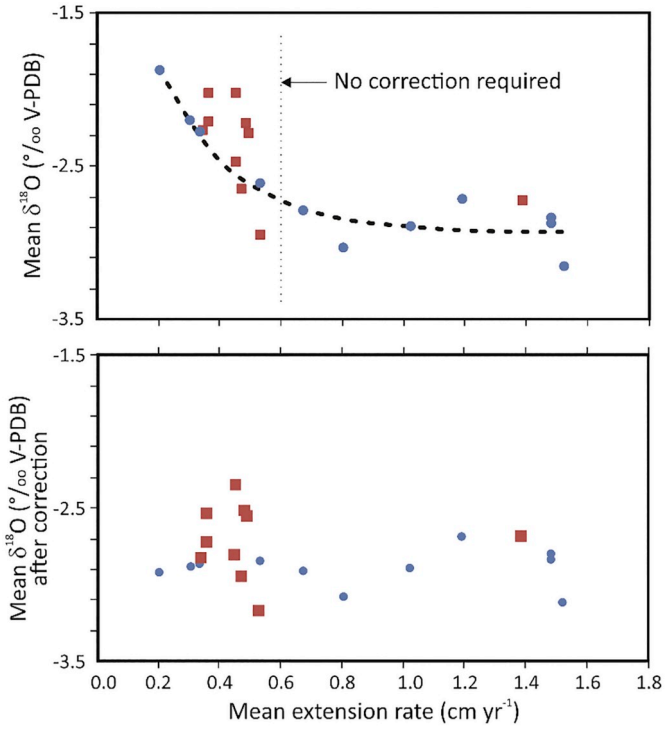

Fig. 8. Mean extension rate versus mean coral $\delta^{18}O_{coral\ calib}$ of massive *Porites* from Psalidha reef site (site 8 from Table 1; red squares) compared to recent *Porites* from the northernmost Red Sea (blue dots). The black dotted line in the upper panel displays an ad hoc best-fit to the modern Red Sea data. The lower panel shows the same data after correction to a common mean extension rate of 1.0 cm yr^{-1}. For extension rates > 0.6 cm yr^{-1}, no correction is required. Red Sea data from Felis et al. (2003).

calcification at three tropical Caribbean sites also, which is incompatible with a cool-water position. Low extension rates of z-corals at tropical fossil sites from the Caribbean have also been reported by other authors (Denniston et al., 2008; Johnson and Pérez, 2006). Bulk $\delta^{13}C$ values are typical for a reef window environment and suggest normal activity of the zooxanthellae (Fig. 6). Interestingly, experimental evidence indicates that corals start producing calcite and grow more slowly in "Cretaceous-type" seawater with a low Mg/Ca ratio (Higuchi et al., 2014; Ries et al., 2006). Nonetheless, no skeletal calcite has been detected by XRD and the biomineralization patterns of scleractinian corals have remained unchanged over the last 40 Ma and before because of a strong physiological control on skeletogenesis (Drake et al., 2020; Janiszewska et al., 2017; Stolarski et al., 2016). Thus, if low Caribbean extension rates are not an effect of high SSTs beyond optimum, factors other than temperature must have interacted efficiently with z-coral skeletal accretion during the past, because no other independent evidence for cool tropics during the Neogene exists to date (Fedorov et al., 2013).

3.4. Evaluating calcification trends: reference and validation data from the Recent

In cross-plots of the 3 calcification variables from the Recent reference and validation datasets, we identify a negative relationship for extension rate and bulk density, however, significant only in the IP (IP: $R^2 = 0.419$, $p < 0.001$; WA-C: $R^2 = 0.039$, $p = 0.472$), while extension rate and calcification rate display highly significant relationships in both, the IP and WA-C (IP: $R^2 = 0.908$, $p < 0.001$; WA-C: $R^2 = 0.699$, $p < 0.001$). A negative correlation between skeletal bulk density and calcification rate exists in the IP ($R^2 = 0.190$, $p < 0.001$), but not so in the WA-C ($R^2 = 0.115$, $p = 0.06$). Nonetheless, the

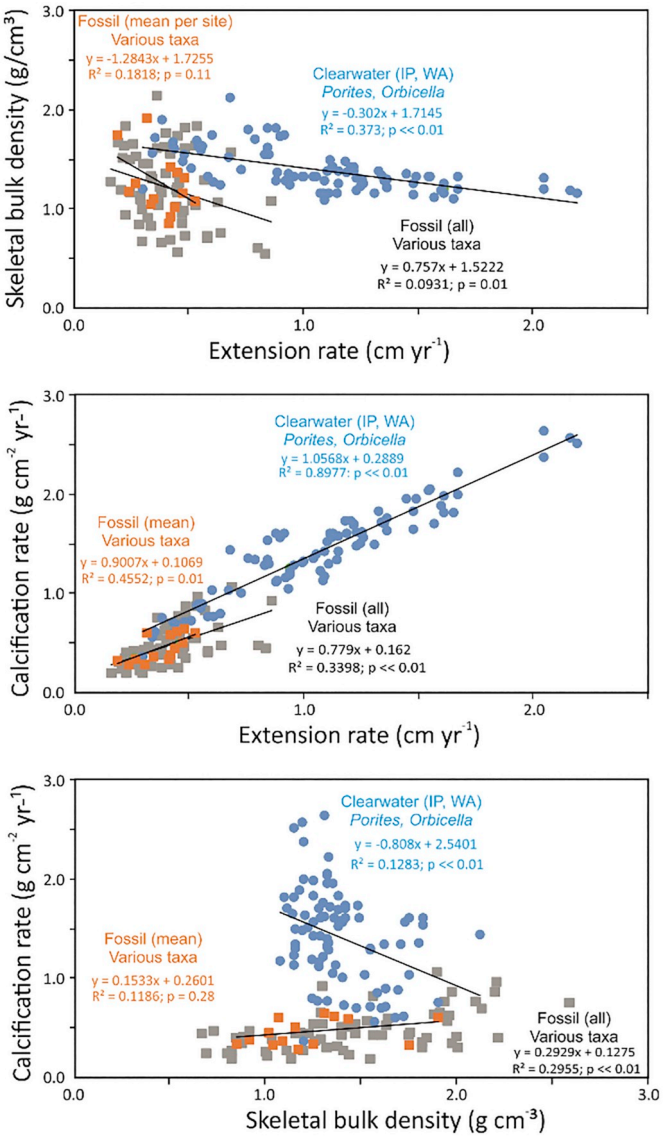

Fig. 9. Calcification systematics of recent and fossil reef corals (averages per site). Blue: recent *Porites* (IP, WA-C) and *Orbicella* (WA-C) from reef-window environment, orange: fossil (various taxa, various environments). Gray: Single specimen mean values for fossil z-corals are shown here for comparison.

regressions and significance of the IP relationships remain highly significant, if the two datasets are pooled (Fig. 9). As a result, the pooled reference and validation datasets allows accurate and consistent predictions of calcification rate to be made from any given extension rate (Equation (1))

$$\text{Calcification rate } (g\ cm^{-2}\ yr^{-1}) = 1.0568\ x\ \text{extension rate } (cm\ yr^{-1}) + 0.2889 \quad (1)$$

We do not use bulk density for making predictions of calcification rate in an analogous way, because uncertainty in the regression is higher due to more scatter in the data. Significantly, mean deviation of the measured values from those predicted by eq. (1) for the IP is 0.0 ± 0.18 g cm^{-2} yr^{-1} for IP *Porites* and 0.0 ± 0.23 g cm^{-3} yr^{-1} for WA-C *Orbicella*, i.e. there is no measurable difference in predicted calcification rate between IP *Porites* and WA-C *Orbicella*.

Qualitative effects of various environmental stresses on the calcification variables from recent and fossil corals are listed in Table 3 and shown in Figures S3–S5. Our findings fully reproduce the results of numerous single studies as reviewed by Lough and Cooper (2011). Earlier studies showed that distance from shore (or exposure to waves) and pH variability in nearshore settings are also important variables for calcification traits on recent reef systems (Crook et al., 2013; Lough and Barnes, 2000; Scoffin et al., 1992). However, these aspects were not recorded as single factors in the dataset because they were hard to infer systematically from the literature for individual growth sites and represent a mix of sediment turbidity and wave exposure, nutrient load and carbon cycling.

3.4.1. The calcification anomaly

As a quantitative measure of calcification performance, we use a new approach that we term calcification anomaly. The calcification anomaly describes the difference between predicted (i.e. from a regression) and measured calcification rate for any given extension rate. A zero calcification anomaly equals optimal calcification within the reef window, while negative and positive anomalies are here termed hypo- and hyper-calcification. As defined here, hypo-calcification (hyper-calcification) has an effect on bulk density being lower (higher) than expected for any given extension rate. The regression equation used for making the predictions derives from the pooled datasets for the reef window environment (clear water) from the IP and WA-C (equation 1). In the reference and validation datasets, clear-water sites symmetrically plot around 0 (optimal calcification). For delineating optimal or hyper- and hypo-calcification, we arbitrarily chose one standard deviation (± 1 SD, i.e. ± 0.17 g cm^{-2} yr^{-1} for the IP and ± 0.23 g cm^{-2} yr^{-1} for the WA-C) from the mean of all data. In practice, we use a simplified definition of ± 0.2 g cm^{-2} yr^{-1} for delimiting optimal calcification from hypo- and hyper-calcification, respectively (Fig. 10). Although the three calcification variables extension rate, bulk density and calcification rate are linked directly to ambient water temperature, the calcification anomaly is a measure of calcification performance independent from SST. It allows calcification performances of symbiotic reef corals to be evaluated where water temperature differs between reef sites and over time, or where water temperature is not sufficiently well known from proxy data.

In the reference and validation datasets, clear-water sites symmetrically plot around 0 (optimal calcification) although the total spread exceeds ± 1 SD (Fig. 10). As predicted, subtropical sites also spread symmetrically around 0, however, hyper-calcified outliers exist. These outliers correspond to *Platygyra daedalea* and *Pavona* sp.. In semi-restricted (elevated salinity) settings, *Platygyra daedalea* also forms hyper-calcified outliers relative to *Porites*, albeit less extreme, likely due to a higher calcification potential than *Porites* (Howells et al., 2018). At volcanic CO_2 vents, calcification is optimal, although shifted towards positive values; at acidic and nutrient-rich freshwater seeps calcification performance is decreased. Deeper-water sites (> 20 m) show optimal calcification, likely because of high water clarity at the sites studied (Red Sea) (Heiss, 1994). Interestingly, corals from turbid environments display a large range of performances; while some sites display no effect of turbidity on calcification, it induces substantial reductions in others. Likely, this is a reflection of qualitative and quantitative differences in turbidity that were not recorded by the dataset (Lough and Cooper, 2011). Upwelling of cold, CO_2-rich water also has strong negative influence on calcification performance, however, records of optimal calcification have been found also in such settings and reflect variable degrees of upwelling intensity and $\Omega_{aragonite}$ (Manzello et al., 2014). Hyper-calcified records are generally rare, but have been documented also in turbid and upwelling sites (single-specimen data only). However, in turbid water this is due to *Platygyra daedalea* having a higher calcification potential than *Porites* (Howells et al., 2018). In upwelling zones, hyper-calcification was recorded through two specimens of *Pavona* sp.. This taxon shows even higher calcification performance in clear-water environments (Fig. 10), suggesting that this taxon has an enhanced calcification potential relative to *Porites* as well. Low calcification performance has been previously reported for *Porites astreoides* (Elizalde-Rendon et al., 2010), but

Table 3
Qualitative dataset results: Recent (IP and WA-C) and fossil environmental effects on skeletal calcification. Given are t- and *p*-values of the *t*-test statistics. n.a. indicates that no data are available. Box plots of the datasets are given in Figs. S3–S5.

		Extension	Density	Calcification rate
Subtropical (rel. to tropical)	Indo-Pacific	7.574; $p \leq 0.001$	-5.621; $p \leq 0.001$	7.128; $p \leq 0.001$
	Western Atlantic	3.433; $p \leq 0.001$	3.332; $p = 0.001$	4.646; $p \leq 0.001$
	fossil	0.65; $p = 0.519$	-1.513; $p = 0.135$	-1.227; $p = 0.224$
Semi-restricted with elevated salinity (rel. to open)	Indo-Pacific	2.281; $p = 0.024$	-4.186; $p \leq 0.001$	1.574; $p = 0.118$
	Western Atlantic	n.a.	n.a.	n.a.
	fossil	1.203; $p = 0.233$	0.695; $p = 0.489$	-1.386; $p = 0.170$
Turbid (rel. to clear water)	Indo-Pacific	-4.204; $p \leq 0.001$	0.101; $p = 0.919$	-4.268; $p \leq 0.001$
	Western Atlantic	-1.759; $p = 0.08$	3.893; $p \leq 0.001$	0.703; $p = 0.484$
	fossil	-1.212; $p = 0.227$	-0.851; 0.397	-1.567; $p = 0.121$
Deep (rel. to shallow)	Indo-Pacific	4.225; $p \leq 0.001$	-2.609; $p = 0.010$	4.495; $p \leq 0.001$
	Western Atlantic	3.996; $p \leq 0.001$	-2.937; $p = 0.004$	3.615; $p \leq 0.001$
	fossil	n.a.	n.a.	n.a.
Upwelling (rel. to stratified)	Indo-Pacific	-0.117; $p = 0.907$	3.475; $p \leq 0.001$	1.297; $p = 0.197$
	Western Atlantic	n.a.	n.a.	n.a.
	fossil	-0.367; $p = 0.715$	4.442; $p \leq 0.001$	2.921; $p = 0.005$
Volcanic vent (CO_2)	Indo-Pacific	0.560; $p = 0.576$	-0.530; $p = 0.597$	0.017; $p = 0.986$
	Western Atlantic	3.064; $p = 0.003$	0.846; $p = 0.399$	3.266; $p = 0.001$
	fossil	n.a.	n.a.	n.a.
Freshwater source (rel. to marine)	Indo-Pacific	-3.302; $p = 0.001$	2.648; $p = 0.009$	-2.207; $p = 0.029$
	Western Atlantic	2.741; $p = 0.007$	5.339; $p \leq 0.001$	6.665; $p \leq 0.001$
	fossil	-0.263; $p = 0.793$	-1.215; $p = 0.229$	-1.282; $p = 0.204$

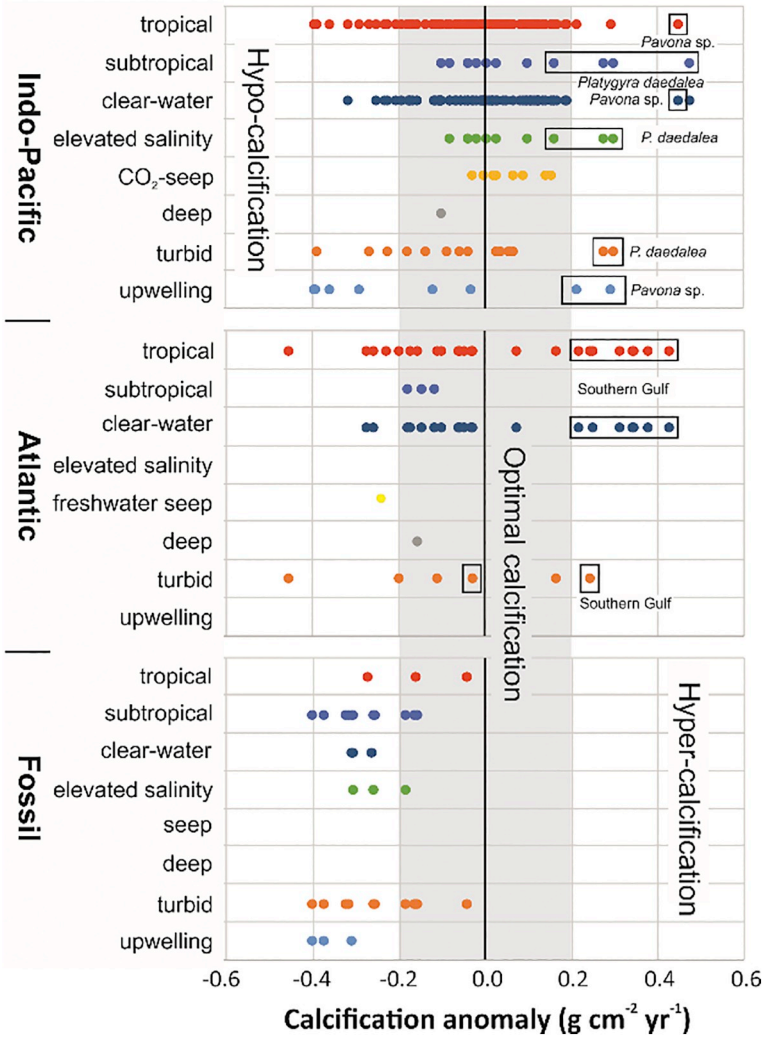

Fig. 10. Diagram showing the calcification anomalies for selected growth environments (mean values per reef site). Top panel: Reference dataset (IP). Middle panel: Validation dataset (WA-C). Bottom panel: Fossil dataset (*Porites*, *Solenastraea*, *Tarbellastraea*, etc, from various regions and Neogene time-slices). Optimal calcification shown as gray bar between ± 0.20 g cm^{-2} yr^{-1}.

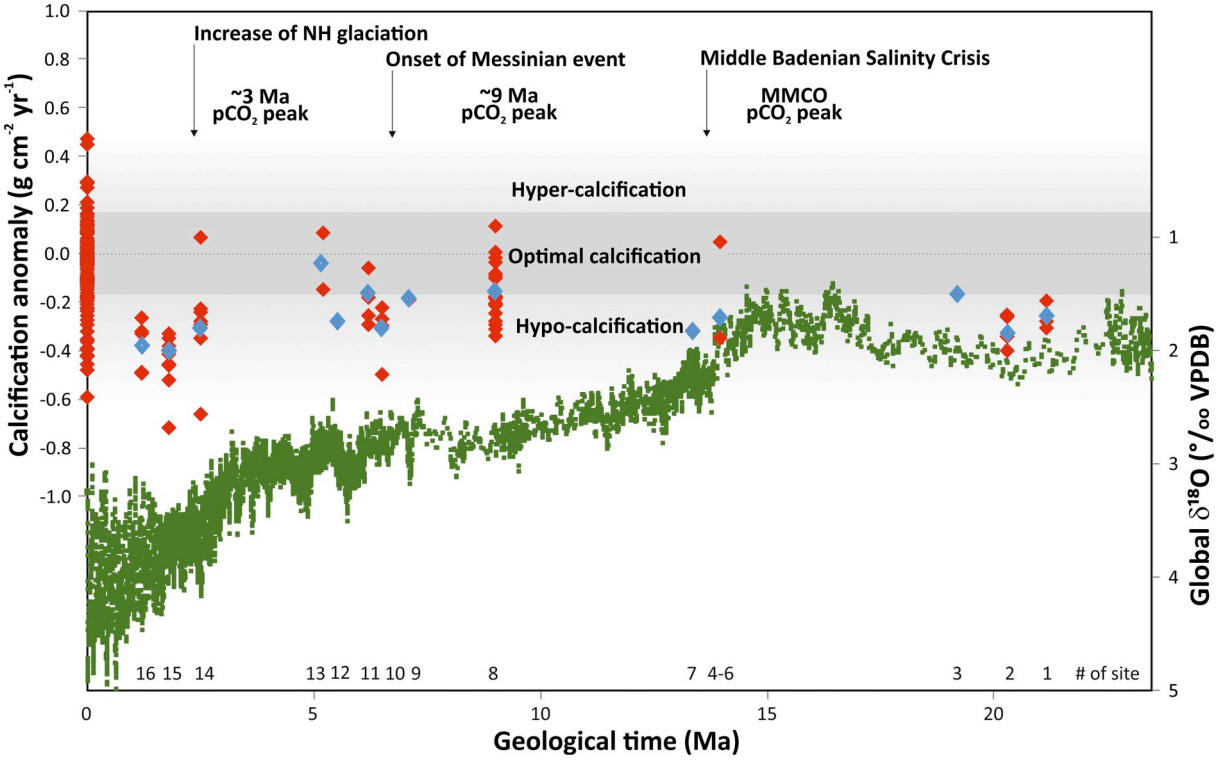

Fig. 11. Diagram showing the calcification anomaly of symbiotic reef corals (upper graph) and global deep-sea oxygen isotope record (lower graph, global $\delta^{18}O$, 5-point running average, from Zachos et al., 2001). Red diamonds show single coral calcification values, blue diamonds means per time-slice. Recent data from Indo-Pacific. NH = Northern Hemisphere, MMCO = Middle Miocene Climatic Optimum. Numbers at the bottom of the diagrams refer to sampling sites as listed in Table 1.

according to our compilation this reflects suboptimal growth environments (turbid water, deep water, freshwater seeping) inducing an inconspicuous negative calcification anomaly that is fully in accord with *Orbicella* at analogous growth sites (Fig. S6). From this discussion we conclude that growth in an optimal reef window-type environment induces optimal calcification, while environmental stress outside the reef growth window causes various degrees of hypo-calcification. Records of hyper-calcification are due to other taxa than *Porites* in the dataset. Hyper-calcification is not likely to occur in *Porites/Orbicella*, because optimal calcification will take place under optimal growth conditions, i.e. the reef growth window (Fig. 10). Hyper-calcification in the WA-C is essentially due to data from the southern Gulf of Mexico; it may reflect enhanced $\Omega_{aragonite}$ due to evaporation in that region (Cai et al., 2010) that is likely to enhance calcification of z-corals (Kleypas et al., 1999a).

3.5. Comparative analysis of the recent and fossil records

The Neogene corals generally display hypo-calcification, whereas optimal calcification or even hyper-calcification virtually do not occur (mean -0.25 ± 0.17 g cm^{-2} yr^{-1}, min. -0.72 g cm^{-2} yr^{-1}, max 0.12 g cm^{-2} yr^{-1}) (Figs. 10, 11). Hypo-calcification implies that the thickening of the early skeletal deposits responsible for extension is incomplete (Lough and Barnes, 2000). It is very unlikely that hypo-calcification during the Neogene was an effect of evolutionary changes of skeletal calcification potentials, because our data derive from extant taxa (except *Tarbellastraea*) and carbon stable isotope data have a typical, zooxanthellate signature at both, sub-annual time-scales and for mean values per corallum (Brachert et al., 2006a; Mertz-Kraus et al., 2008; Roulier and Quinn, 1995) (Fig. 5). The type of algal symbiont controls the tolerance of z-corals against extreme temperature and salinity, but no evidence exists for an effect on calcification potential (Baker et al., 2004; d'Angelo et al., 2015). Furthermore, the corals included in this assessment are in their majority belonging to taxa that display similar, if not identical calcification responses to the environment (*Porites*, *Orbicella*) (Fig. 9, Tab. S1). Therefore, potential changes in the symbiotic system are unlikely to have induced calcification changes over time. Hypo-calcification in the geological past is also not an effect of the subtropical position of most studied sites (Table 1), because water temperature has no strong effect on the calcification anomaly. The same is true for the water depth at the growth site that has no negative effect on calcification according to the calibration datasets (Fig. 10). The fact that our fossil dataset largely samples sites within marginal basins located rather close to shore with turbid water, or upwelling zones etc. (Table 1) implies that most negative calcification anomalies can be explained in terms of the cumulative effects of various, local stressors (Fig. 10). Nonetheless, hypo-calcification rather than optimal calcification was found also at clear-water sites, i.e. reef window-type environments (sites 2, 10, 14; Table 1). Although it is finally unknown whether hypo-calcification is due to too low density for a given extension or due to too low extension rate for a given bulk density (or a combination of both), it is more likely to reflect a too low bulk density for a given extension rate. We come to this conclusion because modern z-corals display the lowest bulk density at sites having the lowest $\Omega_{aragonite}$, and these densities are significantly below those predicted from ambient SST (Manzello et al., 2014). Thus, biomineralization at low sea-water supersaturation with aragonite seems to promote investing calcification resources into extension at the expense of thickening and strengthening (i.e. bulk density) (Mollica et al., 2018). Neogene hypo-calcification at clear-water sites is, therefore, the likely expression of low pH and / or low $\Omega_{aragonite}$ of open seawater. In this respect, it should be noted that one of the clear-water sites was classified also in the category "elevated salinity" (site 10; Table 1) (Fig. 10). Negative growth effects of evaporation and elevated salinity on calcification are not obvious in our reference dataset and were also not reported in the literature (Veron, 2011) (Fig. 10). This is an

interesting aspect, because hypersaline waters have a higher pH and $\Omega_{aragonite}$ than the open ocean (Kleypas et al., 1999a). If these waters were not sufficiently supersaturated with aragonite to support modern-type calcification, reduced pH and carbonate supersaturation of the open ocean is a likely possibility for the time-slices dated 20.8, 20.3, 6.5, and 2.5 Ma (sites 1, 2, 10, 14, Table 1) and supports conclusions from independent proxy data (Sosdian et al., 2018).

Over geological time (16 geological time-slices, plus Recent), calcification performance does not display a clear trend in our dataset, except for a minimum of the anomaly between 3 and 1 Ma and a maximum in the present-day (Fig. 11). Single-coral data at the 3 to 1 Ma calcification minimum display the highest degree of hypo-calcification recorded so far. In this respect, it is interesting to note that the main pulse of extinction of reef corals within the Caribbean region during the Plio-Pleistocene faunal turnover occurred between 2 and 1 Ma and has been linked with increased upwelling and climatic cooling (Budd, 2000; Klaus et al., 2017). Here, we suggest that rapid changes of seawater pH (or $\Omega_{aragonite}$) during the intensification of Northern Hemisphere glaciation dynamics 2.9 to 2.4 Ma ago (Raymo, 1994; Tripati et al., 2011) (Fig. 11) may have been even more important for coral calcification than the cooling itself, because the cooling was essentially a mid and high latitude phenomenon (Fedorov et al., 2013). During this period of time, fluctuations of the CCD at glacial – interglacial time-scales and events of distinct CCD shallowing around ~2 and ~4 Ma together with calcification changes in calcareous plankton document severe re-adjustments of the oceanic carbonate budget (Barker and Elderfield, 2002; Beaufort et al., 2011; Pälike et al., 2012).

3.6. The calcification paradox

For an evaluation of distinct hypo-calcification at sites dated 20.8, 20.3, 6.5 and 2.5 to 1.2 Ma to be an effect of low pH or carbonate starvation of the global ocean, more data from the reef growth window are needed, notably from periods of global warmth such as the MMCO or “mid” Pliocene climate optimum. However, fossil corals fulfilling the criterion of pristine preservation for the analysis of geochemical proxies and calcification variables are generally rare, and their occurrence is typically linked to an embedding in fine-grained, muddy sediments because the associated passive diagenetic environment promotes the preservation of aragonite and original porosity (no dissolution, no cementation) (Longman, 1980). Correspondingly, many specimens used for this review derive from turbid growth settings or debris flow deposits intercalated with basinal mud. Instead, fossil corals from pure carbonate environments of the reef window typically tend to be transformed into stable calcite and fully cemented, because of an active diagenetic environment that promotes dissolution of aragonite and precipitation of calcite (Longman, 1980) (Plate 1). Primary bulk density is destroyed by this process but recrystallized specimens often still display ghost structures of the annual bands (Reuter et al., 2005) (Plate 1/B, D, E). Interestingly, all data available on the spacing of the ghost structures of the annual bands document slow skeletal growth during the Neogene and the last interglacial, irrespective of turbid or clear-water, tropical or subtropical reef environments (Brachert et al., 2006b; Cuevas Miranda et al., 2009; Gischler et al., 2009; Johnson and Pérez, 2006; Shinn, 1966). Hence, it seems there was a general tendency towards low extension rates of z-corals during the late Cenozoic. This overall prevalence of low extension rates implies that calcification rates were low also within the reef growth window, but we cannot say, without ambiguity, whether calcification occurred under optimal reef window-type conditions. With regard to available proxy data for pH and $\Omega_{aragonite}$ (Sosdian et al., 2018), hypo-calcification is most likely to have prevailed at clear-water, reef-window-type sites for most of the past 23 Ma, specifically during the MMCO. In this respect two aspects are interesting to note: (1) Extension rates of z-corals do not drop before undersaturation ($\Omega_{aragonite} < 1$) is reached (Crook et al., 2013), and (2) low extension rates of hypo-calcified corals likely reflect the preferential investment of limited calcification resources into skeletal extension rather than density, because this strategy allows best for reproduction in the overall struggle for light and successful colonization of space on a reef (Fantazzini et al., 2015; Langdon et al., 2000; Tambutté et al., 2015; Veron, 2000). Although it has been proposed that the long-term increase of extension rates in the branching z-coral *Acropora* represents an evolutionary response to increasing rates of sea-level rise from glacial to interglacial during the intensification of the Northern Hemisphere glaciation (Renema et al., 2016), it could equally reflect increasing calcification performance under a long-term declining carbonate starvation regime. Such a resource-limited pattern of calcification during most of the last 23 Ma is in strong contrast to a distributional maximum of coral reefs during climatic optima like the MMCO, however. This paradox of most luxurious reef growth during periods of sustained hypo-calcification in the geological past implies that the present-day´s excessive calcification resources of the reef-window environment could rather be an exception than the norm and the recent is likely no suitable key for understanding the past.

3.6.1. Closing remarks

With this review we have presented an up-to-date overview of the combined records available so far on skeletal calcification of reef corals and stable isotope proxies from the late Cenozoic. Although this work represents a first step towards a better understanding of the evolution of the modern reef system over the last 23 Ma, the data document that the window of sea-surface temperatures remained the same, and some reef growth occurred even within environments with elevated salinity, e.g. the Paratethys prior to the Middle Badenian Salinity Crisis, or the Mediterranean prior to the Messinian Salinity Crisis. Available data are still biased towards subtropical settings, however, and no information is available on what happened with reef corals within the warm pools of the global oceans during climatic extremes, e.g. the MMCO. Nonetheless, the data reveal a tendency towards hypo-calcification of reef corals, and thus support available models and proxy data that predict low pH and low carbonate supersaturation of open ocean waters for most of the late Cenozoic. Many other side-effects on the coral reef ecosystem still need careful consideration, e.g. competition of corals with other reef builders and bioeroders, or changes in global and local paleogeography. Thus, it remains to be solved whether the scenarios described here for the geological past may be good enough for serving as analogues for future developments of global warming and OA. However, the geological record, by its nature, cannot provide any clues as to how the reef systems will react in the future on concomitant anthropogenic disturbances like eutrophication and pollution - aspects that must be taken into account as well in order to assess whether corals will be able to keep up with the ongoing unprecedented speed of global warming, sea-level rise and ocean acidification.

4. Conclusions

1 Fossil z-corals (n = 74) from 16 geological time-slices (20.8 to 1.2 Ma) were reviewed with regard to stable isotope proxies and calcification patterns.
2 Oxygen and carbon stable isotope data document for the most part marine growth environments consistent with subtropical positions in perennially arid and seasonally humid settings or upwelling. Intense evaporative signatures exist in corals from before the MSC in the Mediterranean and the MBSC in the Central Paratethys.
3 Coral sclerochronologies can significantly contribute to our understanding of paleoenvironments. However, low extension rates typical to fossil corals limits their intra-annual resolution and should be taken into account when comparing records of environmental variability, e.g. seasonal SST contrasts.
4 The newly introduced calcification anomaly is a quantitative measure of calcification performance that is independent of SST effects. It allows for comparative assessments of calcification performance

between recent and fossil corals and among corals from different settings. We introduce new terms describing calcification performance: hypo-, hyper-, and optimal calcification.

5 Most fossil corals display hypo-calcification, very few optimal calcification and none hyper-calcification.

6 The degree of hypo-calcification in most fossil specimens is compatible with the cumulative effects of local, nearshore stressors (sediment turbidity, freshwater discharge, upwelling). Corals from four open-oceanic clear-water sites, i.e. reef window-type environments, dated between 20.8 and 1.2 Ma display hypo-calcification as well and point to chronically low pH and / or low $\Omega_{aragonite}$ of ambient waters during the late Cenozoic.

7 The prevalence of hypo-calcified fossils from hypersaline growth environments is unexpected because $\Omega_{aragonite}$ is high in modern hypersaline environments. Hence, it may indirectly reflect low pH and / or low $\Omega_{aragonite}$ of the open ocean at that time.

8 Calcification data from the typical reef growth window environment are available in large numbers for extension rates only. We suggest the known small extension rates of Neogene corals from the reef growth window to reflect skeletogenesis in a regime of global carbonate starvation, in accord with experiments and globally relevant proxy data.

9 Given the concepts of z-coral calcification are correct, the Present is no good key for understanding reef coral calcification and reef growth during the past and future because of an unusually high degree of supersaturation with respect to aragonite.

Author contributions:

TCB designed this study, collected most of the specimens, coordinated the analyses and wrote the paper. MR, TC and LL provided coral specimens and contributed significantly to the manuscript. PS made the density measurements and CW performed the statistics. CP contributed three of the corals, data on their preservation, taxonomy and stratigraphy.

Declaration of Competing Interest

The authors declare that they have no known competing financial interests or personal relationships that could have appeared to influence the work reported in this paper.

Acknowledgements

Janice Lough (AIMS, Townsville, Australia) generously shared with us her files on calcification in modern *Porites* (2013). Frank Bach (Leipzig University, Germany) made fossil specimens from the “Felix Collection” available, and Matthias Harzhauser (Natural History Museum, Vienna, Austria) provided coral specimens from Natural History Museum (Vienna, Austria). The latter colleague is also thanked for his advice on the stratigraphy of the Central Paratethys and for supplying rare historical literature. Jarek Stolarski (Polish Academy of Sciences, Warsaw, Poland) is thanked for his discussion on scleractinian microstructures. We thank an anonymous reviewer and André Strasser (Fribourg University, Switzerland) for their constructive and thoughtful suggestions to improve the manuscript. Wolf-Christian Dullo (Geomar, Kiel, Germany) made many helpful comments on an early version of the manuscript. Gilles Montagnac (ENS Géologie, Lyon) is specially thanked for technical and scientific assistance with Raman microspectromery. XRD and stable isotope analyses were performed by Sylvia Haeßner, Stefan Krüger, Christian Ullmann, and Marlene Höhle (Leipzig University, Germany). Grants by the German Research Foundation (DFG BR1153/13-1 and BR1153/20-1 to TCB) and Austrian Science Fund (FWF P 29158-N29 to MR) are gratefully acknowledged.

Appendix A. Supplementary data

Supplementary data to this article can be found online at https://doi.org/10.1016/j.earscirev.2020.103154.

References

Al-Horani, F.A., 2016. Physiology of skeletogenesis in scleractinian corals. In: Woodley, C.M., Downs, C.A., Bruckner, A.W., Porter, J.W., Galloway, S.B. (Eds.), Diseases of coral. Wiley-Blackwell, Hoboken, pp. 192–205.

Baker, A.C., Starger, C.J., McClanahan, T.R., Glynn, P.W., 2004. Corals' adaptive response to climate change. Nature 430, 741.

Barker, S., Elderfield, H., 2002. Foraminiferal calcification response to glacial-interglacial changes in atmospheric CO_2. Science 297 (5582), 833–836.

Barnes, D.J., Lough, J.M., 1993. On the nature and causes of density banding in massive coral skeleton. J. Exp. Mar. Biol. Ecol. 167, 91–108.

Beaufort, L., Probert, I., de Garidel-Thoron, T., Bendif, E.M., Ruiz-Pino, D., Metzl, N., Goyet, C., Buchet, N., Coupel, P., Grelaud, M., Rost, B., Rickaby, R.E.M., de Vargas, C., 2011. Sensitivity of coccolithophores to carbonate chemistry and ocean acidification. Nature 476 (7358), 80–83.

Benson, B.E., Rippe, J.P., Bove, C.B., Castillo, K.D., 2019. Apparent timing of density banding in the Caribbean coral *Siderastrea siderea* suggests complex role of key physiological variables. Coral Reefs 38 (1), 165–176.

Blanchon, P., 2011. Last interglacial and reef development. In: Hopley, D. (Ed.), Encylopedia of modern coral reefs. Springer, Dordrecht, NL, pp. 621–639.

Böcker, A., 2014. Interannual and seasonal climate variability recorded by reef corals, Plio/Pleistocene (Florida) and Mio/Pliocene (Dominican Republic). In: Dissertation Thesis. Universität Leipzig, Leipzig, pp. 141.

Booker, S., Jones, B., Chacko, T., Li, L., 2019. Insights into sea surface temperatures from the Cayman Islands from corals over the last ~540 years. Sediment. Geol. 389, 218–240.

Brachert, T.C., Betzler, C., Braga, J.C., Martín, J.M., 1996. Record of climatic change in neritic carbonates: Turnovers in biogenic associations and depositional modes (Upper Miocene, southern Spain). Geol. Rundsch. 85, 327–337.

Brachert, T.C., Reuter, M., Felis, T., Kroeger, K.F., Lohmann, G., Micheels, A., Fassoulas, C., 2006a. *Porites* corals from Crete (Greece) open a window into Late Miocene (10 Ma) seasonal and interannual climate variability. Earth Planet. Sci. Lett. 245, 81–94.

Brachert, T.C., Reuter, M., Kroeger, K.F., Lough, J., 2006b. Coral growth bands: A new and easy to use paleothermometer in paleoenvironment analysis and paleoceanography (late Miocene, Greece). Paleoceanography 21, PA4217.

Brachert, T.C., Vescogni, A., Bosellini, F.R., Reuter, M., Mertz-Kraus, R., 2007. High salinity variability during the early Messinian revealed by stable isotope signatures from vermetid and *Halimeda* reefs of the Mediterranean region. Geologica Romana 40, 1–16.

Brachert, T.C., Reuter, M., Krüger, S., Böcker, A., Lohmann, H., Mertz-Kraus, R., Fassoulas, C., 2013. Density banding in corals: barcodes of past and current climate change. Coral Reefs 32, 1013–1023.

Brachert, T.C., Reuter, M., Krüger, S., Kirkerowicz, J., Klaus, J.S., 2016a. Upwelligs mitigated Plio-/Pleistocene heat stress for reef corals on the Florida platform (USA). Biogeosciences 13, 1469–1489.

Brachert, T.C., Reuter, M., Krüger, S., Klaus, J.S., Helmle, K., Lough, J.M., 2016b. Low Florida coral calcification rates in the Plio-Pleistocene. Biogeosciences 13 (15), 4513–4532.

Bruch, A.A., Utescher, T., Mosbrugger, V., members, N, 2011. Precipitation patterns in the Miocene of Central europe and the development of continentality. Palaeogeogr. Palaeoclimatol. Palaeoecol. 304, 202–211.

Budd, A.F., 2000. Diversity and extinction in the Cenozoic history of Caribbean reefs. Coral Reefs 19 (1), 25–35.

Cahuzac, B., Chaix, C., 1996. Structural and faunal evolution of Chattian - Miocene reefs and corals in western France and the Northeastern Atlantic Ocean. In: Franseen, E.K., Esteban, M., Ward, W.C., Rouchy, J.-M. (Eds.), Models for carbonate stratigraphy. From Miocene reef complexes of Mediterranean regions. Concepts in Sedimentology and Paleontology. SEPM, Tusa, pp. 105–127.

Cahuzac, B., Turpin, L., Bonhomme, P., 1997. Sr isotope record in the area of the Lower Miocene historical stratotypus of the Aquitaine Basin. In: Montanari, A., Odin, G.S., Coccioni, R. (Eds.), Miocene stratigraphy - an integrated approach. Developments in Paleontology and Stratigraphy. Elsevier Science, Amsterdam, pp. 33–56.

Cai, W.J., Hu, X., Huang, W.-J., Jiang, L.-Q., Wang, Y., Peng, T.-H., Zhang, X., 2010. Alkalinity distribution in the western North Atlantic Ocean margins. J. Geophys. Res. 115, C08014.

Crook, E.D., Cohen, A.L., Rebolledo-Vieyra, M., Hernandez, L., Paytan, A., 2013. Reduced calcification and lack of acclimatization by coral colonies growing in areas of persistent natural acidification. Proceed. Acad. Nat. Sci. 110 (27), 11044–11049.

Cuevas Miranda, D.N., Sherman, C.E., Ramirez, W., Hubbard, D., 2009. Coral growth rates from the Holocene Cañada Honda fossil reef, Southwestern Dominican Republic: Comparisons with modern counterparts in high sedimentation settings. Caribb. J. Sci. 45 (1), 94–109.

Cuif, J.P., Dauphin, Y., 2005. The Environment Recording Unit in coral skeletons – a synthesis of structural and chemical evidences for a biochemically driven, stepping-growth process in fibres. Biogeosciences 2, 61–73.

Cyronak, T., Schulz, K.G., Jokiel, P.L., 2016. The Omega myth: what really drives lower calcification rates in an acidifying ocean. ICES J. Mar. Sci. 73 (3), 558–562.

d'Angelo, C., Hume, B.C.C., Burt, J., Smith, E.G., Achterberg, E.P., Wiedenmann, J., 2015. Local adaptation constrains the distribution potential of heat-tolerant *Symbiodinium*

from the Persian/Arabian Gulf. ISME J. 2015, 1–10.
Darwin, C., 1842. The geology of the voyage of the Beagle, Part 1: The structure and distribution of coral reefs, London. pp. 214.
De'ath, G., Lough, J.M., Fabricius, K.E., 2009. Declining coral calcification on the Great Barrier Reef. Science 323 (5910), 116–119.
DeCarlo, T.M., Cohen, A.L., 2017. Dissepiments, density bands and signatures of thermal stress in *Porites* skeletons. Coral Reefs 36, 749–761.
DeLong, K.L., 2015. Corals (Sclerochronology). In: Jack Rink, W., Thompson, J.W. (Eds.), Encyclopedia of Scientific Dating Methods. Springer Netherlands, Dordrecht, pp. 187–191.
Denniston, R.F., Penn, S.C., Budd, A.F., 2008. Constraints on Late Miocene shallow marine seasonality for the Central Caribbean using oxygen isotopes and Sr/Ca ratios in a fossil coral. In: Nehm, R.H., Budd, A.F. (Eds.), Evolutionary stasis and change in the Dominican Republic Neogene. Topics in Geobiology. Springer Science and business Media B.V, Heidelberg, pp. 47–63.
Done, T., 2011. Corals: Environmental controls on growth. In: Hopley, D. (Ed.), Encyclopedia of Modern Coral Reefs - Structure, Form and Process. Springer, Dordrecht, NL, pp. 281–293.
Drake, J.L., Mass, T., Stolarski, J., Von Euw, S., van de Schootbrugge, B., Falkowski, P.G., 2020. How corals made rocks through the ages. Global Change Biol. 26, 31–53.
Druffel, E.R.M., 1997. Geochemistry of corals: Proxies of past ocean chemistry, ocean circulation, and climate. Proceed. Nat. Acad. Sci. USA 94, 8354–8361.
Dullo, W.-C., 1984. Progressive diagenetic sequence of aragonite structures: Pleistocene coral reefs and their modern counterparts on the eastern Red Sea coast, Saudi Arabia. Palaeontographica Americana 54 254-160.
Elizalde-Rendon, E.M., Horta-Puga, G., Gonzalez-Diaz, P., Carricart-Ganivet, J.P., 2010. Growth characteristics of the reef-building coral *Porites astreoides* under different environmental conditions in the Western Atlantic. Coral Reefs 29, 607–614.
Enmar, R., Stein, M., Bar-Matthews, M., Sass, E., Katz, A., Lazar, B., 2000. Diagenesis in live corals from the Gulf of Aqaba. I. The effect on paleo-oceanography tracers. Geochim. Cosmochim. Acta 64 (18), 3123–3132.
Fabricius, K.E., Langdon, C., Uthicke, S., Humphrey, C., Noonan, S., De'ath, G., Okazaki, R., Muehllehner, N., Glas, M.S., Lough, J.M., 2011. Losers and winners in coral reefs acclimatized to elevated carbon dioxide concentrations. Nat. Clim. Change 1 (3), 165–169.
Fantazzini, P., Mengoli, S., Pasquini, L., Bortolotti, V., Brizi, L., Mariani, M., di Gosia, M., Fermani, S., Capaccioni, B., Caroselli, E., Prada, F., Zaccanti, F., Levy, O., Dubinsky, Z., Kaandorp, J.A., Konglerd, P., Hammel, J.U., Dauphin, Y., Cuif, J.-P., Weaver, J.C., Fabricius, K.E., Wagermaier, W., Fratzl, P., Falini, G., Goffredo, s., 2015. Gains and losses of coral skeletal porosity changes with ocean acidification. Nature Commun. 6, 7785.
Fedorov, A.V., Brierley, C.M., Lawrence, K.T., Liu, Z., Dekens, P.S., Ravelo, A.C., 2013. Patterns and mechanisms of early Pliocene warmth. Nature 496 (7443), 43–49.
Felis, T., Pätzold, J., 2004. Climate reconstructions from annually banded corals. In: Shiyomi, M., Kawahata, H., Koizumi, H., Tsuda, A., Awaya, Y. (Eds.), Global environmental change in the ocean and on land. Terrapub, Tokyo, pp. 205–227.
Felis, T., Pätzold, J., Loya, Y., Wefer, G., 1998. Vertical water mass mixing and plankton blooms recorded in skeletal stable carbon isotopes of a Red Sea coral. J. Geophys. Res. 103, 30731–30739.
Felis, T., Pätzold, J., Loya, Y., 2003. Mean oxygen-isotope signatures in *Porites* spp. corals: inter-colony variability and correction for extension-rate effects. Coral Reefs 22, 328–336.
Fine, M., Tchernov, D., 2007. Scleractinian coral species survive and recover from decalcification. Science 315 (5820), 1811.
Flügel, E., 2002. Triassic reef patterns. In: Kiessling, W., E, F. (Eds.), Phanerozoic Reef Patterns. SEPM Special Publication. SEPM, Tulsa, pp. 391–463.
Frankowiak, K., Wang, X.T., Sigman, D.M., Gothmann, A.M., Kithahara, M.V., Mazur, M., Meibom, A., Stolarski, J., 2016. Photosymbiosis and the expansion of shallow-water corals. Science Advances 2016 (2), 1–7.
Gattuso, J.-P., Frankignoulle, M., Bourge, I., Romaine, S., Buddemeier, R.W., 1998. Effect of calcium carbonate saturation of seawater on coral calcification. Global and Planetary Change 18 (1-2), 37–46.
Gischler, E., Hudson, J., Storz, D., 2009. Growth of Pleistocene massive corals in south Florida: low skeletal extension-rates and possible ENSO, decadal, and multi-decadal cyclicities. Coral Reefs 28 (4), 823–830.
Glynn, P.W., 1983. Extensive “bleaching” and death of reef corals on the Pacific coast of Panama. 10, 149–154. Environ. Conserv. 10, 149–154.
Goreau, T.F., 1959. The physiology of skeleton formation in corals. I. A method for measuring the rate of calcium deposition by corals under different conditions. Biol. Bull. 116, 59–75.
Gradstein, F.M., Ogg, J.G., Hilgen, F.J., 2012. On the geologic time scale. Newsl. Stratigr. 45 (2), 171–188.
Griffiths, N., Müller, W., Johnson, K.G., Aguilera, O.A., 2013. Evaluation of the effect of diagenetic cements on element/Ca ratios in aragonitic Early Miocene (~16 Ma) Caribbean corals: Implications for "deep-time" palaeoenvironmental reconstructions. Palaeogeogr. Palaeoclimatol. Palaeoecol. 369, 185–200.
Guinotte, J.M., Buddemeier, R.W., Kleypas, J., 2003. Future coral reef habitat marginality: Temporal and spatial effects of climate change in the Pacific basin. Coral Reefs 22, 551–558.
Halley, R.B., Roulier, L.M., 1999. Reconstructing the history of eastern and central Florida Bay using mollusk-shell isotope records. Estuaries 22 (2b), 358–368.
Hallock, P., Schlager, W., 1986. Nutrient excess and the demise of coral reefs and carbonate platforms. Palaios 1, 389–398.
Harzhauser, M., Peckmann, J., Birgel, D., Draganits, E., Mandic, O., Theobaldt, D., Huemer, J., 2014. Stromatolites in the Paratethys during the Middle Miocene climate transition as witness of the Badenian slinity crisis. Facies 60, 429–444.
Heiss, G.A., 1994. Coral reefs in the Red Sea: Growth, production, and stable isotopes. Geomar Rep. 32, 1–141.
Helmle, K.P., Dodge, R.E., Ketcham, R.A., 2002. Skeletal architecture and density banding in Diploria strigosa by X-ray computed tomography. : Proceedings 9th International Coral Reef Symposium, Bali, Indonesia. pp. 365–371 23-27 October 2000, Vol. 1.
Higuchi, T., Fujimura, H., Yuyama, I., Harii, S., Agostini, S., Oomori, T., 2014. Biotic control of skeletal growth by scleractinian corals in aragonite–calcite seas. PLoS ONE 9 (3), e91021.
Hofmann, G.E., Smith, J.E., Johnson, K.S., Send, U., Levin, L.A., Micheli, F., Paytan, A., Price, N.N., Peterson, B., Takeshita, Y., Matson, P.G., Derse Crook, E., Kroeker, K.J., Gambi, M.C., Rivest, E.B., Frieder, C.A., Yu, P.C., Martz, T.R., 2011. High-frequency dynamics of ocean pH: A multi-ecosystem comparison. PLoS ONE 6 (12).
Hönisch, B., Hemming, N.G., Archer, D., Siddall, M., McManus, J.F., 2009. Atmospheric carbon dioxide concentration across the mid-Pleistocene transition. Science 324 (5934), 1551–1554.
Hönisch, B., Ridgwell, A., Schmidt, D.N., Thomas, E., Gibbs, S.J., Slujis, A., Zeebe, R., Kump, L., Martindale, R.C., Greene, S.E., Kiessling, W., Ries, J., Zachos, J.C., Royer, D.L., Barker, S., Marchitto, T.M., Moyer, R., Pelejero, C., Ziveri, P., Foster, G.L., Williams, B., 2012. The geological record of ocean acidification. Science 335, 1058–1063.
Howells, E., Dunshea, G., McParland, D., Vaughan, G., Heron, S., Pratchett, M., Burt, J., Bauman, A., 2018. Species-Specific coral calcification Responses to the extreme environment of the Southern Persian Gulf. Front. Mar. Sci. 5 (56).
Hudson, J.H., Shinn, E.A., Halley, R.B., Lidz, B.H., 1976. Sclerochronology: a tool for interpreting past environments. Geology 4, 361–364.
James, N.P., 1983. Reef environment. In: Scholle, P.A., Bebout, D.G., Moore, C.H. (Eds.), Carbonate Depositional Environments. American Association of Petroleum Geologists Memoir. 33. pp. 345–440 Tulsa, OK.
James, N.P., Bourque, P.-A., 1992. Reefs and mounds. In: Walker, R.G., James, N.P. (Eds.), Facies Models: Response to Sea Level Change. Geological Association of Canada, St. John's, Newfoundland, pp. 323–347.
Janiszewska, K., Mazur, M., Escrig, S., Meibom, A., Stolarski, J., 2017. Aragonitic scleractinian corals in the Cretaceous calcitic sea. Geology 45 (4), 319–322.
Johnson, K.G., Pérez, M.E., 2006. Skeletal extension rates of Cenozoic Caribbean reef corals. Palaios 21, 262–271.
Kiessling, W., Simpson, C., 2011. On the potential for ocean acidification to be a general cause of ancient reef crises. Global Change Biol. 17, 56–67.
Kiessling, W., Flügel, E., Golonka, J., 2002. Phanerozoic Reef Patterns. 72. SEPM Special Publications, SEPM (Society for Sedimentary Geology), Tulsa, pp. 775.
Kitahara, M.V., Cairns, S.D., Stolarski, J., Blair, D., Miller, D.J., 2010. A comprehensive phylogenetic analysis of the Scleractinia (Cnidaria, Anthozoa) based on mitochondrial CO1 sequence data. PLoS ONE 5 (7), e11490.
Klaus, J.S., Meeder, J.F., McNeill, D.F., Woodhead, J.F., Swart, P.K., 2017. Expanded Florida reef development during the mid-Pliocene warm period. Global Planet. Chang.
Kleypas, J.A., Buddemeier, R.W., Archer, D., Gattuso, J.-P., Langdon, C., Opdyke, B.N., 1999a. Geochemical consequences of increased atmospheric carbon dioxide on coral reefs. Science 284 (5411), 118–120.
Kleypas, J.A., McManus, J.W., Menez, L.A.B., 1999b. Environmental limits to coral reef development. Where do we draw the line? Am. Zool. 39, 146–159.
Knutson, D.W., Buddemeier, R.W., Smith, S.V., 1972. Coral chronometers: seasonal growth bands in reef corals. Science 177, 270–272.
Kováč, M., Hudáčková, N., Halásová, E., Kováčová, M., Holcová, K., Oszczypko-Clowes, M., Báldi, K., Less, G., Nagymarosy, A., Ruman, A., Klučiar, T., Jamrich, M., 2017. The Central Paratethys palaeoceanography: a water circulation model based on microfossil proxies, climate, and changes of depositional environment. Acta geologica slovaca 9 (2), 75–114.
Kump, L., Bralower, T., Andy, R., 2009. Ocean acidification in deep time. Oceanography 22.
Langdon, C., Takahashi, T., Sweeney, C., Chipman, D., Goddard, J., 2000. Effect of calcium carbonate saturation on the calcification rate of an experimental coral reef. Global Biogeochemical Cycles 14, 639–654.
Lear, C.H., Coxall, H.K., Foster, G.L., Lunt, D.J., Mawbey, E.M., Rosenthal, Y., Sosdian, S.M., Thomas, E., Wilson, P.A., 2015. Neogene ice volume and ocean temperatures: Insights from infaunal foraminiferal Mg/Ca paleothermometry. Paleoceanography 30 (11), 1437–1454.
Leder, J.J., Swart, P.K., Szmant, A., Dodge, R.E., 1996. The origin of variations in the isotopic record of scleractinian corals: 1 Oxygen. Geochimica et Cosmochim. Acta 60, 2857–2870.
LeGrande, A.N., Schmidt, G.A., 2006. Global gridded data set of the oxygen isotopic composition in seawater. Geophys. Res. Lett. 33 (12) n/a-n/a.
Longman, M.W., 1980. Carbonate diagenetic textures from nearsurface diagenetic environments. American AAPG Bull. 64, 461–487.
Lough, J.M., 2008. Coral calcification from skeletal records revisited. Mar. Ecol. Prog. Ser. 373, 257–264.
Lough, J.M., Barnes, D.J., 2000. Environmental controls on growth of the massive coral

Porites. J. Exp. Mar. Biol. Ecol. 245, 225–243.
Lough, J.M., Cooper, T.F., 2011. New insights from coral growth band studies in an era of rapid environmental change. Earth Sci. Rev. 108, 170–184.
Lozouet, P., Maestrati, P., Favia, R., 2001. Un site exceptionnel du Miocène inférieur (Aquitanien): la `Carrière Vives´ (Meilhan, Landes, France). Bilan de la campagne de fouilles de juillet-aout 1991. Cossmannia 8, 47–67.
Mackenzie, G., Veauvy, C.M., Swart, P.K., Rosen, B.R., Darrell, J.G., 1997. Climatic variation in the early to middle Eocene using the stable oxygen isotopic composition of coral skeletons. Geol. Soc. Am. Abstr. Programs 29 (7) A-395.
Manzello, D.P., Enochs, I.C., Bruckner, A., Renaud, P.G., Kolodziej, G., Budd, D.A., Carlton, R., Glynn, P.W., 2014. Galapagos coral reef persistence after ENSO warming across an acidification gradient. Geophys. Res. Lett. 41, 9001–9008.
McConnaughey, T., 1989. ^{13}C and ^{18}O isotopic disequilibrium in biological carbonates: I. Patterns. Geochim. Cosmochim. Acta 53, 151–162.
McCulloch, M.T., D'Olivo, J.P., Falter, J., Holcomb, M., Trotter, J.A., 2017. Coral calcification in a changing World and the interactive dynamics of pH and DIC upregulation. Nat. Commun. 8, 15686.
McGregor, H.V., Gagan, M.K., 2003. Diagenesis and geochemistry of *Porites* corals from Papua New Guinea: Implications for paleoclimate reconstruction. Geochimica et Cosmochim. Acta 67 (12), 2147–2156.
Mertz-Kraus, R., Brachert, T.C., Reuter, M., 2008. *Tarbellastraea* (Scleractinia): A new stable isotope archive for Late Miocene paleoenvironments in the Mediterranean. Palaeogeogr. Palaeoclimatol. Palaeoecol. 257 (3), 294–307.
Mertz-Kraus, R., Brachert, T.C., Jochum, K.P., Reuter, M., Stoll, B., 2009a. LA-ICP-MS analyses on coral growth increments reveal heavy winter rain in the Eastern Mediterranean at 9 Ma. Palaeogeogr. Palaeoclimatol. Palaeoecol. 273, 25–40.
Mertz-Kraus, R., Brachert, T.C., Reuter, M., Galer, S.J.G., Fassoulas, C., Iliopoulos, G., 2009b. Late Miocene sea surface salinity variability in the Eastern Mediterranean inferred from coral aragonite $\delta^{18}O$ (Crete, Greece). Chem. Geol. 262, 202–216.
Meulenkamp, J.E., Sissingh, W., Calvo, J.P., Daams, R., Londeix, L., Cahuzac, B., Studencka, B., Kovac, M., Marunteanu, M., Nagymarosy, A., Popov, S.V., Scherba, I.G., Roger, J., Platel, J.-P., Hirsch, F., Sadek, A., Abdel-Gawad, G.I., Yaich, C., Bouaziz, S., 2000. Early Burdigalian (20.5 – 19 Ma). In: Dercourt, J., Gaetani, M., Vrielynck, B., Barrier, E., Biju-Duval, B., Brunet, M.F. ... Sandulescu, M. (Eds.), Atlas Peri-Tethys, Palaeogeographical Maps. CCGM/CGMW, Paris, pp. 179–186.
Micheels, A., Bruch, A.A., Eronen, J., Fortelius, M., Harzhauser, M., Utescher, T., Mosbrugger, V., 2010. Analysis of heat transport mechanisms from a Late Miocene model experiment with a fully-coupled atmosphere-ocean general circulation model. Palaeogeogr. Palaeoclimatol. Palaeoecol.
Mollica, N.R., Guo, W., Cohen, A.L., Huang, K.F., Foster, G.L., Donald, H.K., Solow, A.R., 2018. Ocean acidification affects coral growth by reducing skeletal density. In: Proceedings of the Academy of Natural Sciences of Philadelphia, pp. 6.
Pälike, H., Lyle, M.W., Nishi, H., Raffi, I., Ridgwell, A., Gamage, K., Klaus, A., Acton, G., Anderson, L., Backman, J., Baldauf, J., Beltran, C., Bohaty, S.M., BownPaul, Busch. W, Channell, J.E.T., Chun, C.O.J., Delaney, M., Dewangan, P., Dunkley Jones, T., Edgar, K.M., Evans, H., Fitch, P., Foster, G.L., Gussone, N., Hasegawa, H., Hathorne, E.C., Hayashi, H., Herrle, J.O., Holbourn, A., Hovan, S., Hyeong, K., Iijima, K., Ito, T., Kamikuri, S.-i., Kimoto, K., Kuroda, J., Leon-Rodriguez, L., Malinverno, A., Moore Jr, T.C, Murphy, B.H., Murphy, D.P., Nakamura, H., Ogane, K., Ohneiser, C., Richter, C., Robinson, R., Rohling, E.J., Romero, O., Sawada, K., Scher, H., Schneider, L., Sluijs, A., Takata, H., Tian, J., Tsujimoto, A., Wade, B.S., Westerhold, T., Wilkens, R., Williams, T., Wilson, P.A., Yamamoto, Y., Yamamoto, S., Yamazaki, T., Zeebe, R.E., 2012. A Cenozoic record of the equatorial Pacific carbonate compensation depth. Nature 488 (7413), 609–614.
Parize, O., Mulder, T., Cahuzac, B., Fiet, N., Londeix, L., Rubino, J.-L., 2008. Sedimentology and sequence stratigraphy of Aquitanian and Burdigalian stratotypes in the Bordeaux area (southwestern France). Compt. Rendus Geosci. 340, 390–399.
Perrin, C., 2002. Tertiary: The emergence of modern reef ecosystems. In: Kiessling, W., Flügel, E. (Eds.), Phanerozoic Reef Patterns. SEPM Special Publication, Society for Sedimentary Geology, Tulsa, pp. 587–621.
Perrin, C., Bosellini, F.R., 2012. Paleobiogeography of scleractinian reef corals: Changing patterns during the Oligocene–Miocene climatic transition in the Mediterranean. Earth Sci. Rev. 111, 1–24.
Perrin, C., Cuif, J.P., 2001. Ultrastructural controls of diagenetic patterns of scleractinian skeletons: evidence at the scale of colony lifetime. Bull. Tohoku Univ. Museum 1, 210–218.
Perrin, C., Kiessling, W., 2010. Latitudinal trends in Cenozoic reef patterns and their relationsship to climate. Int. Assoc. Sedimentol. Spec. Publ. 42, 17–34.
Perrin, C., Smith, D.C., 2007. Earliest steps of diagenesis in living coral skeletons: evidence from ultrastructural pattern and Raman spectroscopy. J. Sed. Res. 77, 495–507.
Plaziat, J.C., Perrin, C., 1992. Multikilometer-sized reefs built by foraminifera (Solenomeris) from the early Eocene of the Pyrenean domain (S. France, N. Spain): Palaeoecologic relations with coral reefs. Palaeogeogr. Palaeoclimatol. Palaeoecol. 96, 195–231.
Popov, S.V., Rögl, F., Rozanov, A.Y., Steininger, F.F., Shcherba, I.G., Kovac, M., 2004. Lithological-Paleogeographic maps of Paratethys, 10 Maps Late Eocene to Pliocene. Courier Forschungsinstitut Senckenberg (CFS) 250, 1–46.
Quinn, T.M., Taylor, F.W., Crowley, T.J., Link, S.M., 1996. Evaluation of sampling resolution in coral stable isotope records: A case study using records from New Caledonia and Tarawa. Paleocenanography 11, 529–542.
Raymo, M.E., 1994. The initiation of Northern Hemisphere glaciation. Ann. Rev. Earth Pl Sc. 22, 353–383.
Renema, W., Pandolfi, J.M., Kiessling, W., Bosellini, F.R., Klaus, J.S., Korpanty, C., Rosen, B.R.N.S, Wallace, C.C., Webster, J.M., Johnson, K.G, 2016. Are coral reefs victims of their own success? Science Advances 2 (4) e1500850.
Reuter, M., Brachert, T.C., Kroeger, K.F., 2005. Diagenesis of growth bands in fossil scleractinian corals: Identification and modes of preservation. Facies 51, 155–168.
Riegl, B., Bruckner, A., Coles, S.L., Renaud, P., Dodge, R.E., 2009. Coral Reefs. In: Threats and Conservation in an Era of Global Change, The Year in Ecology and Conservation Biology. Ann. N.Y. Acad. Sci. New York Academy of Sciences, New York, pp. 136–186.
Ries, J.B., Stanley, S.M., Hardie, L.A., 2006. Scleractinian corals produce calcite, and grow more slowly, in artificial Cretaceous seawater. Geology 34, 525–528.
Ries, J.B., Cohen, A.L., McCorkle, D.C., 2009. Marine calcifiers exhibit mixed responses to CO2-induced ocean acidification. Geology 37 (12), 1131–1134.
Romano, S.L., Cairns, S.D., 2000. Molecular phylogenetic hypotheses for the evolution of scleractinian corals. Bull. Mar. Sci. 67 (3), 1043–1068.
Romano, S.L., Palumbi, S.R., 1996. Evolution of scleractinian corals inferred from molecular systematics. Science 271 (5249), 640–642.
Rosen, B.R., 2000. Algal symbiosis, and the collapse and recovery of reef communities: Lazarus corals across the K–T boundary. In: Culver, S.J., Rawson, P.F (Eds.), Biotic Response to Global Change: The Last 145 Million Years. Cambridge University Press, Cambridge, pp. 164–180.
Roulier, L.M., Quinn, T.M., 1995. Seasonal- to decadal-scale climatic variability in southwest Florida during the middle Pliocene: Inferences from a coralline stable isotope record. Paleoceanography 10 (3), 429–443.
Scheibner, C., Speijer, R.P., 2008. Decline of coral reefs during late Paleocene to early Eocene global warming. eEarth 3, 19–26.
Schroeder, J.H., Purser, B.H. (Eds.), 1986. Reef Diagenesis. Springer-Verlag, New York, pp. 448.
Scoffin, T.P., Tudhope, A.W., Brown, B.E., Chansang, H., Cheeney, R.F., 1992. Environmental controls of *Porites lutea*, south Thailand. Coral Reefs 11, 1–13.
Seki, O., Foster, G.L., Schmidt, D.N., Mackensen, A., Kawamura, K., Pancost, R.D., 2010. Alkenone and boron-based Pliocene pCO_2 records. Earth Planet. Sci. Lett. 292, 201–211.
Shinn, E.A., 1966. Coral growth-rate, an environmental indicator. J. Paleontol. 40, 233–240.
Sierro, F.J., Flores, J.A., Francés, G., Vazquez, A., Utrilla, R., Zamarreno, I., Erlenkeuser, H., Barcena, M.A., 2003. Orbitally controlled oscillations in planktic communities and cyclic changes in western Mediterranean hydrography during the Messinian. Paleogeogr. Paleoclimatol. Paleoecol. 190, 289–316.
Sosdian, S.M., Greenop, R., Hain, M.P., Foster, G.L., Pearson, P.N., Lear, C.H., 2018. Constraining the evolution of Neogene ocean carbonate chemistry using the boron isotope pH proxy. Earth Planet. Sci. Lett. 498, 362–376.
Stanley, G.D., 2003. The evolution of modern corals and their early history. Earth Sci. Rev. 60, 195–225.
Stanley Jr, G., van de Schootbrugge, B., 2018. The evolution of the coral–algal symbiosis and coral bleaching in the geologic past. In: van Oppen, M.J.H., Lough, J.M. (Eds.), In: Coral Bleaching Patterns, Processes, Causes and Consequences. Springer, Amsterdam, pp. 9–26.
Stanley, G.D., Swart, P.K., 1995. Evolution of the coral-zooxanthellae symbiosis during the triassic: A geochemical approach. Paleobiology 21, 179–199.
Stolarski, J., 2003. Three-dimensional micro- and nanostructural characteristics of the scleractinian coral skeleton: A biocalcification proxy. Acta Palaeontol. Pol. 48 (4), 497–530.
Stolarski, J., Bosellini, F.R., Wallace, C.C., Gothmann, A.M., Mazur, M., Domart-Coulon, I., Gutner-Hoch, E., Neuser, R.D., Levy, O., Shemesh, A., Meibom, A., 2016. A uniquie coral biomineralization pattern has resisted 40 million years of major ocean chemistry change. Sci. Rep. 6 (27579).
Swart, P.K., 1983. Carbon and oxygen isotope fractionation in scleractinian corals: A review. Earth Sci. Rev. 19, 51–80.
Swart, P.K., Healy, G.F., Dodge, R.E., Kramer, P., Hudson, J.H., Halley, R.B., Robblee, M.B., 1996. The stable oxygen and carbon isotopic record from a coral growing in Florida Bay: a 160 year record of climatic and anthropogenic influence. Palaeogeogr. Palaeoclimatol. Palaeoecol. 123, 219–237.
Tambutté, E., Venn, A.A., Holcomb, M., Segonds, N., Techer, N., Zoccola, D., Allemand, D., Tambutte, S., 2015. Morphological plasticity of the coral skeleton under CO_2-driven seawater acidification. Nature Commun 6.
Tripati, A.K., Roberts, C.D., Eagle, R.A., Li, G., 2011. A 20 million year record of planktic foraminiferal B/Ca ratios: Systematics and uncertainties in pCO_2 reconstructions. Geochimica et Cosmochim. Acta 75 (10), 2582–2610.
Tudhope, A.W., Lea, D.W., Shimmield, G.B., Chilcott, S., Head, S., 1996. Monsoon climate and Arabian sea coastal upwelling recorded in massive corals from southern Oman. Palaios 11 (4), 347–361.
Veron, J.E.N., 2000. Corals of the world, 1. Australian Institute of Marine Science, Townsville.
Veron, J.E.N., 2011. Coral: Biology, skeletal deposition, and reef-building. In: Hopley, D. (Ed.), Encyclopedia of modern coral reefs - structure, form and process. Springer, Dordrecht, NL, pp. 275–281.
Watanabe, T., Suzuki, A., Minobe, S., Kawashima, T., Kameo, K., Minoshima, K., Aguilar, Y.M., Wani, R., Kawahata, H., Sowa, K., Nagai, T., Kase, T., 2011. Permanent El Nino

during the Pliocene warm period not supported by coral evidence. Nature 471 (7337), 209–211.
Weiss, T.L., Denniston, R.F., Wanamaker, A.D., Villarini, G., von der Heydt, A.S., 2017. El Niño–Southern Oscillation–like variability in a late Miocene Caribbean coral. Geology 1–4.
White, C.H., Bosence, D.W.J., Rosen, B.R., Wallace, C.C., 2008. Response of *Acropora* to warm climates; lessons from the geological past. In: 11th International Coral Reef Symposium, Ft. Lauderdale, pp. 7–12.
Wilson, J.L., 1975. Carbonate Facies in Geologic History. Springer Verlag, New York, pp. 471.
Wilson, M.E.J., Rosen, B.R., 1998. Implications of paucity of corals in the Paleogene of SE Asia: plate tectonics or Centre of Origin? In: Hall, R., Holloway, J.D. (Eds.), Biogeography and Geological Evolution of SE Asia. Backhuys, Leiden, pp. 165–195.
Wood, R.A., 1999. Reef Evolution. Oxford Univ. Press, Oxford.
Worum, F.P., Carricart-Ganivet, J.P., Besnon, L., Golicher, D., 2007. Simulation and observation of annual density banding in skeletons of *Montastrea* (Cnidaria: Scleractinia) growing under thermal stress associated with ocean warming. Limnol. Oceanogr. 52 (2), 2317–2323.
Zachos, J., Pagani, M., Sloan, L., Thomas, E., Billups, K., 2001. Trends, rhythms, and aberrations in global climate 65 Ma to present. Science 292, 686–693.